Key drivers of ozone change and its radiative forcing over the 21st century

Fernando Iglesias-Suarez[1,2,*], Douglas E. Kinnison[3], Alexandru Rap[4], Amanda C. Maycock[4], Oliver Wild[1,2] and Paul J. Young[1,2,5]

[1]Lancaster Environment Centre, Lancaster University, Lancaster, UK

[2]Data Science Institute, Lancaster University, Lancaster, UK

[3]Atmospheric Chemistry Observations and Modeling Laboratory, National Center for Atmospheric Research, Boulder, Colorado, USA

[4]School of Earth and Environment, University of Leeds, Leeds, UK

[5]Pentland Centre for Sustainability in Business, Lancaster University, Lancaster, UK

[*]now at: Department of Atmospheric Chemistry and Climate Group, Institute of Physical Chemistry Rocasolano, CSIC, Madrid, Spain

Correspondence to: F. Iglesias-Suarez (figlesias@iqfr.csic.es)

Abstract

Over the 21st century changes in both tropospheric and stratospheric ozone are likely to have important consequences for the Earth's radiative balance. In this study, we investigate the radiative forcing from future ozone changes, using the Community Earth System Model (CESM1), with the Whole Atmosphere Community Climate Model (WACCM), and including fully coupled radiation and chemistry schemes. Using year 2100 conditions from the Representative Concentration Pathways 8.5 (RCP8.5) scenario, we quantify the individual contributions to ozone radiative forcing of (1) climate change (with and without lightning feedback), (2) reduced concentrations of ozone depleting substances (ODSs), and (3) methane increases. We calculate future ozone radiative forcings relative to year 2000 of (1) 33 ± 104 mWm^{-2}, (2) 163 ± 109 mWm^{-2}, and (3) 238 ± 113 mWm^{-2}, due to climate change, ODSs and methane, respectively. Our best estimate of net ozone forcing in this set of simulations is 430 ± 130 mWm^{-2} relative to year 2000, and 760 ± 230 mWm^{-2} relative to year

1750, with the 95 % confidence interval given by ±30 %. We find that the overall long-term tropospheric ozone forcing from methane chemistry-climate feedbacks related to OH and methane lifetime is relatively small (46 mWm^{-2}). Ozone radiative forcing associated with climate change and stratospheric ozone recovery are robust with regard to background climate conditions, even though the ozone response is sensitive to both changes in atmospheric composition and climate. Changes in stratospheric-produced ozone account for ~50 % of the overall radiative forcing for the 2000–2100 period in this set of simulations, highlighting the key role of the stratosphere in determining future ozone radiative forcing.

1 Introduction

Ozone is an important trace gas that plays a key role in the Earth's radiative budget, atmospheric chemistry and air quality. As a radiatively active gas, ozone interacts with both shortwave and longwave radiation. In the troposphere, ozone is an important regulator of the oxidising capacity (both itself and as the main source of hydroxyl radicals, OH), as well as being an important pollutant, with negative effects on vegetation and human health (e.g. Prather et al., 2001; UNEP, 2015). However, approximately 90% of ozone by mass is found in the stratosphere – protecting the biosphere from harmful ultraviolet solar radiation (WMO, 2014) – and is an important source of ozone in the troposphere and its budget (e.g. Collins et al., 2003; Sudo et al., 2003; Zeng and Pyle, 2003). Therefore, its future evolution – in the troposphere and the stratosphere – is an important concern for climate change and air quality during the 21st century. Future changes in emissions of ozone precursors (e.g. methane), ozone depleting substances (ODSs) and climate are thought to be major drivers of ozone abundances (e.g. Stevenson et al., 2006; Kawase et al., 2011; Young et al., 2013; Banerjee et al., 2016).

Stratospheric-tropospheric exchange (STE) of ozone significantly influences the abundance and distribution of tropospheric ozone (e.g. Zeng et al., 2010; Banerjee et al., 2016). The Brewer-Dobson circulation (BDC) governs the meridional transport of air and trace constituents in the stratosphere, and is characterized by upwelling in the tropics, poleward motion in the stratosphere and sinking at middle and high latitudes (Butchart, 2014, and references therein). The BDC is commonly thought to

consist of a shallow branch, controlling the lower stratosphere region, and a deep branch controlling the middle and upper stratosphere. The latter presents two cells during the spring and fall seasons, and one stronger cell into the winter hemisphere (Birner and Bönisch, 2011). Although observational estimates and climate models suggest an acceleration of the stratospheric mean mass transport via the BDC associated with climate change (e.g. Oberländer et al., 2013; Ploeger et al., 2013; Butchart, 2014; Stiller et al., 2017), significant uncertainty still remains (Engel et al., 2009; Hegglin et al., 2014; Ray et al., 2014). The tropopause is the boundary that "separates" the troposphere and the stratosphere, two chemically and dynamically distinct regions. Defining the tropopause is crucial to diagnose budget terms of trace gases such as the STE of ozone (e.g. Prather et al., 2011), although the chosen definition may affect the resulting analysis (e.g. Wild, 2007; Stevenson et al., 2013; Young et al., 2013).

Stratospheric ozone is expected to recover towards pre-industrial levels during the 21st century due to the implementation of the Montreal Protocol and its Amendments and Adjustments (WMO, 2014), as ODS concentrations slowly decrease in the atmosphere (e.g. Austin and Wilson, 2006; Eyring et al., 2010). Indeed, the global ozone layer has already shown the first signs of recovery (WMO, 2014; Chipperfield et al., 2017). Future ozone recovery can affect tropospheric composition via enhanced STE of ozone and reductions in tropospheric photolysis rates, both associated with higher levels of ozone in the stratosphere. Previous modelling studies that have isolated the impacts of stratospheric ozone recovery have shown that the increased STE is the most important driver of changes in the tropospheric ozone burden (Zeng et al., 2010; Kawase et al., 2011; Banerjee et al., 2016). However, tropospheric ozone is also significantly affected by the change in ultraviolet radiation reaching the troposphere brought about by the ticker stratospheric ozone layer. In turn, reductions in ozone photolysis result in lower OH concentrations – i.e. $O_3 + h\nu\ (\lambda < 320\ \text{nm}) \rightarrow O(^1D) + O_2$ – and therefore longer methane lifetime, with consequences for long-term tropospheric ozone abundances (e.g. Morgenstern et al., 2013; Zhang et al., 2014).

The broad impacts of future climate change on the distribution of ozone are robust across a number of modelling studies and multi-model activities (Kawase et al., 2011; Young et al., 2013; Arblaster et al., 2014; Banerjee et al., 2016; Iglesias-Suarez

et al., 2016). Stratospheric cooling leads to further ozone loss in the polar lower stratosphere (through enhanced heterogeneous ozone destruction) and ozone increases in the upper stratosphere (through reduced NO_x abundances and HO_x-catalysed ozone loss, and enhanced net oxygen chemistry) (Haigh and Pyle, 1982; Rosenfield et al., 2002). In addition, a projected acceleration of the BDC leads to an enhanced STE of ozone (e.g. Garcia and Randel, 2008; Butchart et al., 2010), which results in (i) decreases in tropical lower stratospheric ozone, associated with a relatively faster ventilation and reduced ozone production (Avallone and Prather, 1996); and (ii) ozone increases in the upper troposphere, particularly in the region of the subtropical jets, linked to the descending branch of the BDC (e.g. Kawase et al., 2011; Banerjee et al., 2016). On the other hand, a warmer and wetter climate results in reduced tropospheric ozone levels – i.e. linked to a decrease in net chemical production due to enhanced ozone chemical loss – (e.g. Wild, 2007).

Climate feedbacks associated with future ozone changes are surrounded by large uncertainties. Lightning is a major natural source of nitrogen oxides (LNO_x) in the troposphere (Galloway et al., 2004), with important consequences for atmospheric composition in the mid-upper troposphere and the lower stratosphere. The current best estimate of annual and global mean LNO_x emissions is 5 ± 3 Tg(N) yr^{-1}, with chemistry-climate models suggesting LNO_x emissions sensitivity to climate change of $\sim 4–60$ % K^{-1} (Schumann and Huntrieser, 2007, and references therein). Although more recent modelling studies find LNO_x emissions climate sensitivity lying at the lower end of the above estimate (Zeng et al., 2008; Banerjee et al., 2014), results from a multi-model activity suggest large uncertainty in the magnitude and even the sign of future projections response due to different parameterizations (Finney et al., 2016). Most LNO_x emissions occur in the mid-upper tropical troposphere over the continents, where photochemical production of ozone is most efficient in the troposphere – i.e. low background concentrations and longer lifetimes of NO_x, lower temperatures affecting ozone loss chemistry and abundant sunlight (e.g. Williams, 2005; Dahlmann et al., 2011). A small but significant fraction of lightning-induced NO_x emissions are converted into less photochemically active nitric acid (HNO_3, via HO_2 + NO reaction), which can be removed through wet deposition or transported into the lower stratosphere (acting as a reservoir of NO_x) (e.g. Jacob, 1999; Søvde et al., 2011). In addition, OH concentrations increase with LNO_x emissions and the

resultant lightning-produced ozone – i.e. via NO + HO_2 and $O(^1D)$ + H_2O respectively – with a corresponding reduction in methane lifetime. This resulting climate feedback is important because methane is a potent greenhouse gas (GHG) and ozone precursor.

To date, ozone is the third largest contributor to the total tropospheric radiative forcing (RF) since the pre-industrial period, with overall increases in its concentration contributing a global radiative forcing over 1750–2011 of +0.35 Wm^{-2} (Myhre et al., 2013). In this study, we use the concept of radiative effect (RE) to diagnose the contribution of ozone changes on the global radiative budget. The ozone RE is the radiative flux imbalance between incoming shortwave solar radiation and outgoing longwave infrared radiation (at the tropopause, after allowing for stratospheric temperatures to re-adjust to radiative equilibrium), which results from the presence of both anthropogenic and natural ozone (Rap et al., 2015). Note that RF is therefore the change in RE over time (e.g. Myhre et al., 2013). Ozone shows two distinct regimes with regard to its RE, with positive (longwave radiation) and negative (shortwave radiation) effects for increases in stratospheric ozone, and positive (for both longwave and shortwave radiation) effects for ozone increases in the troposphere (e.g. Lacis et al., 1990; Forster and Shine, 1997). In addition, changes in the distribution of ozone – i.e. latitudinal and vertical structure – are of a particular interest for its RE, due to horizontally varying factors such as, surface albedo, clouds and the thermal structure of the atmosphere (e.g. Lacis et al., 1990; Berntsen et al., 1997; Forster and Shine, 1997; Gauss et al., 2003). Previous studies showed highest radiative efficiency of ozone in the tropical upper troposphere (e.g. Worden et al., 2011; Riese et al., 2012; Rap et al., 2015), a region greatly influenced by changes in stratospheric influx (e.g. Hegglin and Shepherd, 2009; Zeng et al., 2010; Banerjee et al., 2016) and lightning-produced ozone (e.g. Banerjee et al., 2014; Liaskos et al., 2015) in a warmer climate.

Modelling experiments used in the latest Assessment Report of the Intergovernmental Panel on Climate Change (IPCC) followed the Representative Concentration Pathways (RCPs) emission scenarios for short-lived precursors (van Vuuren et al., 2011) and long-lived species (Meinshausen et al., 2011). The RCPs are named according to the total radiative forcing at the end of the 21st century relative to 1750. For example, while the RCP8.5 emissions scenario refers to the total 8.5 Wm^{-2} RF by 2100, future tropospheric ozone RF was projected to account for up to ~9 % (0.6 ± 0.2 Wm^{-2}) of the total RF (Stevenson et al., 2013). Note that the methane

concentration in 2100 is more than double that in the year 2000 following the RCP8.5 emissions scenario.

Previous research has investigated impacts on ozone abundances and distributions associated to future changes in climate, ODSs and ozone precursor emissions in a processed-based approach – i.e. imposing one single forcing at a time – (Collins et al., 2003; Sudo et al., 2003; Zeng and Pyle, 2003; Zeng et al., 2008; Zeng et al., 2010; Kawase et al., 2011; Banerjee et al., 2016). Other modelling studies focused on the radiative effects of tropospheric (e.g. Gauss et al., 2003; Stevenson et al., 2013) and stratospheric (Bekki et al., 2013) ozone changes under future emission scenarios in a non processed-based fashion. One study has recently identified the indirect tropospheric and stratospheric ozone RF between 2000 and 2100 due to individual perturbations (Banerjee et al., 2018). Yet the upper limit of future ozone RF remains poorly constrained. For example, climate models do not even necessarily agree on the sign of the indirect ozone forcing resulting from climate change and associated feedbacks (e.g. LNO_x). Furthermore, there are uncertainties arising from the interactions and non-linearities between different agents (e.g. combined forcing may differ from the sum of individual forcings due to different background conditions), as well as and long-term changes (e.g. methane feedback associated with changes in lifetimes).

Here we aim to narrow this gap by assessing how key factors drive net ozone radiative forcing, and providing an estimate of the uncertainty arising from non-linearities and long-term feedbacks. We use the Community Earth System Model (CESM1) in its "high-top" (up to 140 km) atmosphere version – the Whole Atmosphere Community Climate Model (WACCM) – and a series of sensitivity simulations to quantify the radiative effects of ozone due to (1) climate change, (2) lightning-induced NO_x emissions, (3) stratospheric ozone recovery, and (4) methane emissions between 2000 and 2100 following the RCP8.5 emissions scenario. We explore the robustness of the ozone radiative forcings associated with the above drivers under different background conditions due to non-linearities in ozone responses. Moreover, here we use a synthetic ozone tracer to unambiguously identify stratospheric- and tropospheric-produced ozone forcing. Note this study does not address reductions in anthropogenic NO_x and non-methane volatile organic

compounds emissions, since they play a marginal role in future ozone RF under the RCP8.5 scenario (based on an additional simulation not presented here).

The CESM1-WACCM model, sensitivity simulations and ozone radiative effect calculations are described in Section 2. A present-day model evaluation, future projected ozone changes and associated radiative effects are presented in Sect. 3. Different sources of uncertainties are discussed and accounted for in Sect. 4. Finally, a summary and concluding remarks are presented in Sect. 5.

2 Methodology

2.1 Model description

We use the CESM (version 1.1.1) chemistry-climate model with a configuration that fully couples the atmosphere and land components. A comprehensive description of the model is given by Marsh et al. (2013, and references therein).

The atmosphere component of CESM is WACCM version 4, a high-top model that extends from the surface to approximately 140 km in the lower thermosphere, with a vertical resolution ranging from 1.2 km near the tropopause to ~ 2 km near the stratopause, and horizontal resolution of 1.9º x 2.5º (latitude by longitude). The chemical scheme is the Model for Ozone and Related Chemical Tracers (MOZART) for the troposphere (Emmons et al., 2010) and the stratosphere (Kinnison et al., 2007), including recent updates (Lamarque et al., 2012; Tilmes et al., 2015). It includes 169 chemical species with detailed photolysis, gas-phase and heterogeneous reactions (see Tables A1 and A2 in Tilmes et al., 2016). Recent updates in the orographic gravity wave forcing – reducing the cold bias in Antarctic polar temperatures – (Calvo et al., 2017; Garcia et al., 2017) and the polar stratospheric chemistry (Wegner et al., 2013; Solomon et al., 2015) are included in the model. Concentrations of radiatively active gas-phase compounds such as ozone, nitrous oxide (N_2O), methane (CH_4) and halogenated ODSs, are coupled to the model radiation scheme. Lightning-induced NO_x (LNO_x) emissions are parameterized using the cloud top height method (Price and Vaughan, 1993), and annual global mean LNO_x emissions are scaled to simulate present-day values of between 3–5 Tg N yr^{-1}.

A stratospheric ozone tracer (O3S) is implemented to represent the abundance and distribution of stratospheric-produced ozone in the troposphere (Roelofs and Lelieveld, 1997). O3S is equivalent to ozone in the stratosphere. In the troposphere it undergoes the same chemical loss processes as ozone, but does not undergo dry deposition, following the recommendations for the Chemistry-Climate Model Initiative (CCMI) (Eyring et al., 2013; Morgenstern et al., 2017). To account for dry deposition of O3S, we apply an annual global correction factor based on an additional model simulation (not used in the main results). This correction factor is approximately linear, ranging from 0.7 at the surface to 0.95 around 250 hPa.

The land component is the Community Land Model version 4, which has the same horizontal resolution as the atmosphere component and interactively calculates dry deposition for trace gases in the atmosphere (Val Martin et al., 2014) and biogenic emissions using the Model of Emissions of Gases and Aerosols from Nature (MEGAN) version 2.1 (Guenther et al., 2012).

2.2 Experimental setup

This modelling set-up uses time slice simulations driven by sea surface temperatures (SSTs) and sea ice climatologies from previous CESM1-WACCM fully coupled simulations performed as part of the CCMI (SENC2-8.5; see Morgenstern et al., 2017). An average over 1990-2009 is used to represent the year 2000; since the existing model simulation did not cover the period 2090-2109, an average over 2080-2099 is used to represent conditions at the end of the 21st century (nominally 2100). Note, however, that the perturbed concentrations of atmospheric gases are taken from year 2100 in the RCP8.5 scenario, and hence these experiments are labelled as 2100 in the manuscript. Each time slice experiment is integrated for 20 years, with the last 10 years analysed in this study (i.e. the spin-up period covered the first 10 years). Seasonally varying boundary conditions are specified for carbon dioxide (CO_2), N_2O, CH_4, and ODSs (halogen-containing compounds), as recommended for CCMI (Eyring et al., 2013). Changes in ozone precursors – other than CH_4 – and land-use changes are not explored here (i.e. these are fixed at year 2000 levels in all experiments). Volcanic eruptions are not included in the experiments, and the incoming solar radiation is fixed at 1361 Wm^{-2}. The quasi-biennial oscillation is imposed by

relaxation of equatorial winds (90–3 hPa) with an approximate 28-month period between eastward and westward phases (Marsh et al., 2013).

Table 1 lists the simulations used in this study. The control simulation (Cnt) had all boundary conditions set to the year 2000. Then each sensitivity simulation added one single driver (i.e. boundary condition changed to the year 2100) at a time. For example, while the climate-related ozone RF (with fixed LNO_x emission) is explored comparing the Clm−Cnt simulations, the forcing associated with changes in lightning-induced NO_x emissions is quantified comparing the Lnt−Clm simulations, and so forth. This method provides a different estimate of the overall net ozone RF compared to exploring the impact of the individual drivers alone (e.g. it accounts for non-linear effects that may be neglected by exploring each perturbation compared to the reference simulation). However, since the attribution of forcings to individual drivers may be sensitive to different background conditions, we also evaluate the robustness of the experimental design (see Sect. 3.5).

Here we provide specific details of the boundary conditions. The simulations can be classified into three main groups:

1. Sensitivity simulations that explore the impacts of climate change. Here SSTs, sea ice and main GHGs (i.e. CO_2 and N_2O) are specified to year 2100 levels (see above for explanation of SST and sea ice fields). The upper end emission scenario of the RCPs family is explored (RCP8.5). Natural biogenic emissions (e.g. isoprene) are calculated online, which are mainly governed by changes in CO_2, climate and land use (Squire et al., 2014). The indirect ozone radiative effect resulting from this climate feedback is implicitly contained in the climate signal. However, unlike LNO_x emissions it mainly impacts ozone in the lower troposphere, where ozone shows relatively small radiative efficiency (Rap et al., 2015). To isolate the impacts of lightning-produced ozone, additional experiments are performed with year 2000 levels for LNO_x emissions (fLNOx). Fixed LNO_x simulations follow the approach of Banerjee et al. (2014), imposing the monthly mean LNO_x emissions climatology from the Cnt run and switching off its interactive calculation in the model. To justify this method, we compared temperature and tropospheric ozone fields between the Cnt and Cnt+fLNOx simulations and found negligible differences (not shown).

2. Stratospheric ozone recovery due to the slow decrease of ODS concentrations (referring to the total organic chlorine and bromine species) regulated under the framework of the Montreal Protocol is investigated. Based on the CCMI recommendations, halogen species (CFC11, CFC12, CFC113, CFC114, CFC115, CCl4, HCFC22, HCFC141b, HCFC142b, CF_2ClBr, CF_3Br, CH_3Br, CH_3CCl_3, CH_3Cl, H1202, H2402, CH_2Br_2, and $CHBr_3$) are specified to year 2100 levels for the halogen scenario A1 (WMO, 2011), which includes the early phase-out of hydrochlorofluorocarbons agreed in 2007. Note that two brominated short-lived species (CH_2Br_2 and $CHBr_3$) were included in these experiments to accurately represent bromine loading and thus the associated ozone depletion, providing an additional bromine surface mixing ratio of ~ 6 pptv on top of that from the longer-lived bromine compounds.
3. Future levels of methane and its impacts on ozone are investigated. Concentrations of CH_4 are imposed to year 2100 levels from the RCP8.5 pathway – i.e. approximately double concentrations compared to year 2000. Note that methane levels were kept at year 2000 levels for the sensitivity simulations described above that explore climate change impacts.

2.3 Radiative transfer calculations

To calculate the resulting all-sky REs of ozone we use the ozone radiative kernel (O_3 RK) technique based on Rap et al. (2015), updated for the whole atmosphere (Figure 1). The O_3 RK, defined as the derivative of the radiative flux relative to small perturbations in ozone, was calculated using the offline version of the SOCRATES radiative transfer model with nine longwave (LW) and six shortwave (SW) bands, which is based on Edwards and Slingo (1996). Radiative flux calculations employed a monthly mean climatology of temperature, water vapour and ozone from the European Centre for Medium-Range Weather Forecast (ECMWF) ERA-Interim, and year 2000 surface albedo and clouds from the International Satellite Cloud Climatology Project (Rossow and Schiffer, 1999). Stratospherically adjusted REs of ozone were computed using the fixed dynamical heating approximation (Fels et al., 1980), which assumes that the atmosphere adjusts to a new equilibrium state via radiative process only – i.e. without dynamical feedbacks – on a relatively short period (~ few months). A 1 ppb perturbation in ozone is added to each layer in turn,

and temperatures above 200 hPa are adjusted iteratively until they converge to a new local radiative-dynamical equilibrium and the change in net flux at the 200 hPa level is diagnosed. The O_3 RK is then constructed from the changes in net flux resulting from the ozone perturbations applied to all atmospheric layers. The 200 hPa level is used for the stratospheric temperature adjustment as an approximation for the level at which the transition to local radiative-dynamical equilibrium in the stratosphere occurs. The net O_3 RK (Fig. 1a) illustrates the importance of the upper troposphere and lower stratosphere, particularly at low latitudes, where changes in ozone are very efficient in affecting the radiative flux of the Earth. The LW component (Fig. 1b) is positive throughout the atmosphere and dominates the net O_3 RK, although the SW component (Fig. 1c) outweighs the former in the upper stratosphere (i.e. negative sensitivity).

We compared the ozone RF calculated using the O_3 RK technique (i.e. by multiplying the simulated ozone change with the net O_3 RK interpolated to the model's grid) with the corresponding RF calculated directly with the SOCRATES radiative transfer model (see supplementary material, Fig. S1). The good agreement between the two methods (global mean difference of 0.01 Wm^{-2}) is consistent with the Rap et al. (2015) findings, where the O_3 RK was proposed as an efficient and accurate method to estimate ozone RFs, which is particularly well suited for multi-model intercomparison activities.

A chemical tropopause definition (Prather et al., 2001), using the 150 ppb ozone level of the Cnt simulation, is employed to differentiate ozone changes and associated RFs occurring in the troposphere and the stratosphere. Compared to the latter, we found a negligible difference in the partitioning of tropospheric-stratospheric forcing using a consistent chemical tropopause definition to the driver investigated (i.e. higher tropopause associated with climate change).

3 Results

3.1 Present-day ozone radiative effects and model validation

A detailed present-day ozone evaluation of a similar model and experimental set-up was presented by Tilmes et al. (2016). In summary, simulated monthly mean ozone

shows good agreement with observational estimates within a 25 % range in spring and summer. Zonal and annual mean tropospheric ozone shows the best agreement with observations at low and mid-latitudes (±5 DU), a key region for its radiative effect (e.g. Rap et al., 2015). Likewise, the zonal and annual mean stratospheric ozone agrees fairly well with satellite estimates in the Southern Hemisphere (SH) and low latitudes (±30 DU), but larger deviations are found at mid- and high latitudes in the Northern Hemisphere (NH), a discrepancy also apparent in the models of the Atmospheric Chemistry and Climate Model Intercomparison Project (ACCMIP) (Iglesias-Suarez et al., 2016). The tropospheric ozone budget (production, loss, dry deposition, stratospheric input), burden and lifetime for the Cnt simulation (see Table 2 and Fig. S2) are within previous multi-model activities estimates (Stevenson et al., 2013; Young et al., 2013; Young et al., 2018).

Figures 2a-2b show the annual mean ozone RE calculated for the Cnt simulation (year 2000 or "present-day" hereafter) and the Tropospheric Emission Spectrometer (TES) from July 2005 until June 2008 (05–08). TES is the first product providing tropospheric ozone profiles suitable for RE studies and has been previously evaluated against other observational estimates (e.g. Osterman et al., 2008), showing small bias in the troposphere and the stratosphere of approximately 3–4 DU. The annual and global ozone RE in the Cnt simulation is 2.26 ± 0.14 Wm^{-2} (1 standard error associated with interannual variability), within the TES range of 2.21–2.26 Wm^{-2}. The spatial distribution of simulated and observed ozone REs are fairly well correlated (r = 0.6, $p < 0.01$), although note that the noisier TES signal is largely the result of averaging only three years. Both the simulated and observed present-day ozone REs reveal a positive poleward gradient, with a minimum in tropical regions (approximately 20ºN-20ºS) that is associated with the relatively low ozone levels found in the upper troposphere and lower stratosphere (see Fig. S2). A peak is found at high latitudes in the NH, driven by transport of relatively rich tropospheric ozone air from mid-latitudes coupled with only moderate ozone depletion in the NH stratosphere. This is in contrast with a lower RE values within the SH polar vortex, driven by the larger stratospheric ozone depletion over Antarctica (Solomon et al., 2015). Figure 2c compares the Cnt annual mean ozone RE against the TES data set. Compared to TES, the simulated annual mean tends to overestimate the RE in the NH and underestimate it in the SH, consistent with the bias in the ozone

distribution (Tilmes et al., 2016). Significant biases are mainly confined to the tropical and subtropical regions – i.e. bias is defined here when the simulated RE ±1.96 standard error (~95 % confidence interval) is outside the observed range. Although tropical and subtropical regions are of particular interest for future changes in ozone and its resulting radiative forcing (i.e. highest radiative efficiency), there is a large NH/SH compensation as shown by the annual and global mean forcings. Note the RE is the radiative flux imbalance at a given time due to a radiatively active species (e.g. with and without ozone), whereas the RF refers to the change in RE over time.

3.2 Ozone changes

Figure 3 shows modelled annual and zonal mean ozone changes by 2100 compared to present-day. We present results from adding one single perturbation at a time.

Climate (Clm−Cnt; Fig. 3a) shows similar pattern of ozone response to that found previously (e.g. Kawase et al., 2011; Banerjee et al., 2014). In the troposphere, ozone decreases primarily as a consequence of a warmer and more moist climate, which drives increased ozone loss via an enhanced $O(^1D) + H_2O$ flux (Johnson et al., 2001). Reduced net chemical production is partially offset by an increase in the STE (Table 2), driven by an enhanced BDC (Zeng and Pyle, 2003). The fingerprint of this change in the BDC can be seen in the lower stratosphere, both for decreases in the tropics and increases at mid-latitudes, respectively associated with the enhanced ascending and descending regions (Hegglin and Shepherd, 2009). In this simulation, the 70 hPa tropical (20°N-20°S) and zonal mean upwelling (Andrews et al., 1987) increases by 3.4 % dec^{-1} compared to Cnt (100 year trend). This trend is in agreement with current climate models projections of ~3.2 ± 0.7 % dec^{-1} between 2005–2099 following the RCP8.5 (Hardiman et al., 2014). Additional ozone depletion over the Antarctic is consistent with stratospheric cooling due to enhanced GHG levels (Fig. S4a), driving enhanced heterogeneous ozone loss chemistry (WMO, 2014). In contrast, cooling in the upper stratosphere results in ozone increases associated with a slowdown of catalytic O_x cycles (Haigh and Pyle, 1982; Rosenfield et al., 2002).

Future lightning (Lnt−Clm; Fig. 3b) shows an increase in LNO_x emissions by ~33 %, which results in ozone increases mainly in the tropical and subtropical upper troposphere. However, present-day LNO_x emissions have significant uncertainties and

climate models do not agree even on the sign of the change due to different lightning parameterizations (Finney et al., 2016). Nevertheless, the simulated present-day LNO_x emissions of 4.8 ± 1.6 Tg(N) yr^{-1} lies within observationally-derived estimates, and the model's LNO_x sensitivity to climate of 10.8 % K^{-1} is at the upper end of the two standard deviation climate model range (8.8 ± 2 % K^{-1}) (Finney et al., 2016). The net global tropospheric ozone responses to climate will be largely determined by the interplay between (non-lightning) climate-induced ozone losses and lightning-induced ozone production.

Reductions in inorganic chlorine and bromine abundances (O3r−Ltn; Fig. 2c) result in stratospheric ozone increases. Upper stratospheric ozone recovers largely due to decreases in ClO_x-catalysed ozone destruction. Due to reduced heterogeneous ozone loss chemistry, the largest changes are found in polar regions in the lower stratosphere, with increases of ~450 % over the Antarctic (November) and ~45 % over the Arctic (April). Greater abundances of stratospheric ozone result in an approximately 20 % increase in the STE (Table 2) driving higher levels of tropospheric ozone, particularly at mid- and high latitudes in the SH (related to ozone hole recovery) and tropical and subtropical upper troposphere (the descending region of the BDC), which is consistent with previous model estimates (Banerjee et al., 2016). The BDC-driven increases are somewhat offset by the larger overhead ozone column reducing actinic fluxes and therefore ozone photochemical production (Table 2) (Banerjee et al., 2016).

Methane is a greenhouse gas, an ozone precursor in the troposphere and plays various roles in the stratosphere, and these processes are difficult to isolate from the rest. Future methane (Mth−O3r; Fig. 3d) emissions show a widespread increase of ozone in the troposphere, with annual and global tropospheric column ozone increase of 15 ± 8 % (Table S1). Previous modelling studies reported similar increases of 10–13 % (Brasseur et al., 2006; Kawase et al., 2011). Compensation between ozone decreases in the upper stratosphere (enhanced HO_x-catalysed chemistry) and increases in the lower stratosphere (smog-like chemistry and the partitioning of active/inactive chlorine) (Randeniya et al., 2002; Stenke and Grewe, 2005; Portmann and Solomon, 2007; Fleming et al., 2011; Revell et al., 2012), results in small changes of 2 ± 5 % for the annual and global stratospheric column ozone.

3.3 Ozone radiative forcing

Figure 4 shows maps of annual mean radiative forcing between 2000 and 2100 due to changes in ozone for the whole atmosphere, along with zonal mean forcings associated with changes in the troposphere and the stratosphere for single perturbation simulations. Note that zonal mean forcings are weighted by latitudinal area (i.e. cosine-latitude), allowing direct comparison with the total forcing. Annual and global mean forcing values and their standard error (i.e. due to ozone changes only) are listed in Table 3. Ozone radiative forcing shows strong dependence on the vertical distribution of the change (e.g. Lacis et al., 1990; Forster and Shine, 1997; Rap et al., 2015) and to a lesser extent on the horizontal distribution (e.g. Berntsen et al., 1997). Differences can be seen in both the geographical pattern of the forcing and in the magnitude related to the drivers.

The global forcing associated with climate (Clm−Cnt; Fig. 4a) of −70 ± 102 mWm^{-2} is relatively small and not highly statistically significant (errors denote 1 standard error associated with the 10 year interannual variability of ozone change unless otherwise specified). The geographical pattern shows a relatively strong and significant forcing at high latitudes in the NH, related to ozone increases in the lower stratosphere (transport from enhanced BDC) and upper stratosphere (reduced chemical loss due to cooling). However, this is outweighed by a negative tropospheric forcing in the tropics and a negative stratospheric forcing in the SH extra-tropical region. The latter is largely due to additional ozone depletion in the lower stratosphere (i.e. reduction of STE; not shown).

Future lightning-induced NO_x emissions (Ltn−Clm; Fig. 4b) shows relatively large though not significant global ozone forcing of 104 ± 108 mWm^{-2}, mainly the result of simulated tropospheric ozone changes of 2.1 ± 2.3 DU. Two distinct peak regions are evident around the subtropical belts, where large ozone changes are coincident with relatively cloud-free areas, higher temperature, and a low solar zenith angle. The strongest positive forcing is found over the Sahara and Middle East deserts, associated with greater surface albedo.

Ozone recovery (O3r−Ltn; Fig. 4c) drives a significant forcing of 163 ± 109 mWm^{-2}. This forcing is largely confined to the mid- and high latitudes, particularly in the SH (due to ozone hole recovery), and is mainly linked to the

stratosphere. Extra-tropical STE is especially important in the SH. This is demonstrated by tropospheric forcing of about ~100 mWm^{-2} in this region, which is largely the result of stratospheric-produced ozone transported to the troposphere.

Methane emissions show a large positive forcing around the subtropical belts (Mth−O3r; Fig. 4d), which is principally confined to the troposphere, as there is a compensation between changes in the lower and upper stratosphere (Fig. 3d). In the tropical and subtropical troposphere, methane is more readily oxidised partly associated with higher OH levels, which results in relatively large ozone increases (Fig. 3d). In addition, significant forcings at high latitudes, particularly over the Arctic, are linked to the stratosphere (i.e. reduced ozone loss via decreased active/inactive chlorine partitioning).

Figure 5 shows maps of annual mean normalised tropospheric ozone radiative forcing (NRF) between 2000 and 2100 for the four sensitivity simulations. The NRF – defined here as the tropospheric ozone radiative forcing divided by the tropospheric column ozone – is a useful diagnostic to gain insight into radiative effects of ozone changes. Very similar global NRFs of ~39 mWm^{-2} DU^{-1} due to (non-lightning) climate and methane, indicates relatively evenly distributed ozone changes in the troposphere. In contrast, more localised lightning-produced ozone results in higher global NRF of 46 mWm^{-2} DU^{-1}, whereas ozone increases at high latitudes due to ozone recovery results in smaller NRF of 35 mWm^{-2} DU^{-1}. This highlights the dependence of the resulting forcings on the vertical and horizontal distribution of changes in ozone.

Previous studies have shown that the radiative forcing from tropospheric and stratospheric ozone do not have distinct drivers (Søvde et al., 2011; Shindell et al., 2013). Our results support this and show that climate change, ODSs and methane have consequences for both tropospheric and stratospheric ozone radiative forcing (Table 3). In this set of simulations, changes in ozone occurring in the troposphere and the stratosphere respectively contribute ~70 % and 30 % to the total annual and global forcing of 435 ± 108 mWm^{-2}.

Further insight can be gained by attributing ozone forcing based on its origin in the stratosphere or the troposphere. In these simulations, we used a stratospheric ozone tracer (see Sect. 2) to unambiguously differentiate ozone with tropospheric

origin (O3T) from that with stratospheric origin (O3S). Table 3 shows such "source classified" ozone radiative forcings, using the "O3S/ozone" and "O3T/ozone" ratios for tropospheric and stratospheric forcings respectively. Stratospheric-produced ozone contributes to ~50 % of the annual and global future ozone forcing in this set of simulations, which strongly reinforces the importance of stratospheric-tropospheric interactions.

3.4 Methane feedback and resulting ozone forcing

Future climate change and emissions of ODSs and methane will affect the oxidising capacity of the atmosphere (e.g., via hydroxyl radicals, OH), which influences the methane lifetime (τCH_4) and its concentration. In turn, changes in methane concentrations result in a "long-term" response of tropospheric ozone at decadal time scales (e.g. Fuglestvedt et al., 1999; Wild and Prather, 2000; Holmes et al., 2013). The simulations considered here neglect this feedback by imposing fixed and uniform lower boundary conditions for methane. However, we can estimate how methane concentrations would have adjusted if they were free to evolve, as well as the associated ozone response and radiative forcing. Using the method described by Fiore et al. (2009, and refences therein), we calculate global mean equilibrium methane abundances, $[CH_4]_{eq}$, by

$$[CH_4]_{eq} = [CH_4]_{Cnt} \times \left(\frac{\tau CH_4(p)}{\tau CH_4(r)}\right)^{f} \quad (1)$$

where Cnt represents the fixed boundary conditions for year 2000; *(p)* and *(r)* refer to the perturbation and reference simulations respectively; and f is a feedback factor which accounts for the response of methane to its own lifetime. The feedback factor is explicitly calculated for WACCM using the O3r "(a)" and Mth "(b)" simulations, as follows

$$f = \frac{1}{(1-s)} \quad (2)$$

where s is calculated by

$$s = \frac{[\ \ln(\ \tau CH_4(b)\ ) - \ln(\ \tau CH_4(a)\ )]}{[\ \ln(\ BCH_4(b)\ ) - \ln(\ BCH_4(a)\ )]} \quad (3)$$

and where BCH_4 is the annual and global mean methane burden. We calculate a value of f of 1.43 which is at the upper end of the literature range (1.19–1.53) (Prather et al., 2001; Stevenson et al., 2013; Voulgarakis et al., 2013) but within 7 % of the observationally constrained best estimate of 1.34 (Holmes et al., 2013).

The ozone response to this methane feedback is estimated by linear interpolation:

$$\Delta O3(\mathrm{eq} - \mathrm{Cnt}) = \left[\frac{\Delta CH_4(\mathrm{eq} - \mathrm{Cnt})}{\Delta CH_4(\mathrm{b} - \mathrm{a})}\right] \times \Delta O3(\mathrm{b} - \mathrm{a}) \quad (4)$$

where ΔO3 is the change in annual and global mean of tropospheric column ozone (Table S1). Assuming the relationships between changes in methane, ozone and radiative forcings are linear; the associated tropospheric ozone forcings to methane feedback are given by the product of ΔO3 and the NRF due to methane perturbation (39 mWm^{-2} DU^{-1}; Fig. 5d) and are shown in Table 3. The overall long-term tropospheric ozone forcing related to the methane feedback in this set of simulations is a moderate increase of ~15 %. Climate change (Clm and Ltn simulations) enhances the oxidising capacity of the atmosphere, which results in a small negative forcing of −19 mWm^{-2} due to the methane feedback. In the Mth simulation, OH concentrations are strongly reduced and the associated forcing of 63 mWm^{-2} outweighs the climate forcing. This forcing is within the range of ~40–120 (mean value of 60) mWm^{-2} from the ACCMIP ensemble (Table 8 in Stevenson et al., 2013), when considering the same change in methane concentrations (note their values have been linearly extrapolated).

3.5 Background conditions and forcing

Since the ozone response to a given perturbation is dependent on the background conditions (e.g. temperature, radiative heating, trace gas levels), the resulting forcing associated to individual drivers may be sensitive to the experimental design. For example, lightning-induced ozone forcing due to climate change may differ significantly under present-day or doubled methane concentrations (i.e. year 2000 or year 2100-RCP8.5 abundances). In the present study, we imposed single perturbations successively. Therefore, the total ozone forcing calculated from this set of simulations

includes chemistry-climate feedbacks arising from the interactions between the various perturbations. Yet the attribution of indirect ozone forcings to individual drivers may be sensitive to the order considered (Table 1).

We also completed an additional set of simulations (Table S2) to assess the robustness of the calculated RF to the order the perturbations were applied (Table 3). Lightning-induced net ozone forcing (104 ± 108 mWm^{-2} from Table 3) is not significantly different at the 95 % confidence interval (due to interannual variability only unless otherwise specified) compared to that calculated under approximately doubled methane concentrations (Ltn_Mth−Clm_Mth). Although the reported lightning net ozone forcing is 50 mWm^{-2} lower relative to the latter, both lie within the interannual uncertainty (~100 mWm^{-2}). The forcing associated with ozone recovery (163 ± 109 mWm^{-2}) is calculated under climate change (i.e. including lightning feedbacks) and present-day methane concentrations, though it also can be derived under present-day climate (O3r_Ods−Cnt) or doubled methane concentrations (Mth−Ltn_Mth). We find no significant differences between the forcings associated with these background conditions, although the reported mean forcing resulting from ozone recovery is greater by ~30 mWm^{-2}. Finally, methane-induced net ozone forcing due to doubling its concentrations relative to present-day under ozone recovery conditions (238 ± 113 mWm^{-2}), is not significantly different to that under present-day ODS concentrations (Ltn_Mth−Ltn) or without lightning feedbacks (Clm_Mth−Clm). The reported forcing associated with methane lies within the latter forcings (i.e. 50 mWm^{-2} range). Therefore, we conclude that future ozone forcings due to lightning, ozone recovery and methane concentrations – presented in Table 3 – are robust, with regard to background conditions.

The fact that global and annual ozone forcings associated with single perturbations are not significantly different with regard to background conditions is perhaps somewhat surprising, given that, for instance, ozone production is sensitive to the relative abundances of volatile organic compounds and NO_x (e.g. Sillman, 1999). However, while the globally averaged forcing is not significantly affected by the order in which the perturbations are considered, there are significant differences in budget terms (e.g. ozone burden differences due to lightning can be as large as 4.5 ± 1.4 Tg), as well as ozone levels in particular regions of the atmosphere.

Therefore, the non-linear additivity of the perturbations is important when considering their impacts on quantities such as ozone profiles and surface air quality (not shown).

4 Uncertainties and outlook

We calculate a net ozone radiative forcing of 435 ± 108 mWm^{-2} corresponding to the year 2100 under the RCP8.5 emissions scenario compared to present-day, with the one standard error uncertainty arising from variability in ozone between the years of the time slice simulations. This variability indicates a ±25 % uncertainty, which is slightly larger than the spread across the ACCMIP ensemble of approximately ±20 % (Stevenson et al., 2013). However, additional sources of uncertainty exist in the ozone forcing. Previously, uncertainties arising from the tropopause definition (±3 %), the radiation scheme or forcing calculation (±10 %), and the extent to which clouds and stratospheric temperature adjustment influence ozone forcing (±7 % and ±3 % respectively) have been estimated (Stevenson et al., 2013). Climate feedbacks, land-use change, natural ozone precursor emissions, and future changes in the structure of the tropopause (Wilcox et al., 2012) may introduce at least an additional ±20 % uncertainty (Stevenson et al., 2013). Following Stevenson et al. (2013), we assume that the above individual uncertainties are independent and combine them to estimate an overall uncertainty of ±30 %, which represents the 95 % confidence interval. We note that Skeie et al. (2011) from an independent analysis estimated the same overall uncertainty.

Figure 6 summarises the global and annual net ozone forcing as well as the forcings by driver and region. Overall, our annual global mean best estimate for the net ozone radiative forcing between 2000 and 2100 is 430 ± 130 mWm^{-2}, with tropospheric and stratospheric forcings of 300 ± 90 mWm^{-2} and 130 ± 40 mWm^{-2}, respectively. Current estimates for tropospheric and stratospheric ozone forcings from 1750 to 2011 are 400 ± 20 mWm^{-2} and −50 ± 100 mWm^{-2}, respectively (Myhre et al., 2013). An increase of 0.5 DU in tropospheric ozone was estimated in Skeie et al. (2011) from 2000 to 2010, and a tropospheric ozone normalized radiative forcing of 42 mWm^{-2} DU^{-1} calculated from the ACCMIP ensemble (Stevenson et al., 2013). Therefore, we estimate a net ozone forcing of 760 ± 230 mWm^{-2} from 1750 to 2100 based on our simulations, which is the result of the forcings in the troposphere and the

stratosphere (690 ± 210 mWm^{-2} and 70 ± 20 mWm^{-2} respectively). Our tropospheric forcing is within the range estimated from the ACCMIP models of 600 ± 120 mWm^{-2} (Table 12 in Stevenson et al., 2013).

Previous work has shown that NRF is an appropriate tool for estimating annual and global tropospheric forcings derived from changes in tropospheric column ozone, which in turn reduces the multi-model uncertainty (Gauss et al., 2003). The NRF in our analysis of 43 mWm^{-2} DU^{-1} is similar to that from the ACCMIP models between the 1850s and 2000s, but larger compared to that in Gauss et al. (2003). This supports the future tropospheric ozone forcings and their uncertainties during the 21st century derived from the ACCMIP ensemble (calculated using the NRF), and may be used as a benchmark for individual studies.

Although previous studies have examined key drivers of ozone during the 21st century and future changes are relatively well understood (e.g. Kawase et al., 2011; Banerjee et al., 2014; Banerjee et al., 2016), the resulting forcings have been explored in less detail (e.g. Gauss et al., 2003; Bekki et al., 2013; Stevenson et al., 2013). Following a process-based approach that includes chemistry-climate feedbacks, we calculate that climate-only, lightning, ozone recovery and methane emissions contribute respectively −16 ± 24 %, 24 ± 25 %, 38 ± 25 %, and 55 ± 26 % to the net ozone RF between 2000 and 2100 (Table 3 and Fig. 6). Further uncertainties arise from the long-term ozone response to methane changes, which could increase the overall tropospheric forcing by ~15 %. Climate change (including lightning feedbacks) alone produces a relatively small tropospheric ozone forcing of 64 ± 44 mWm^{-2}. A subset of eight models from the ACCMIP activity shows a small negative but not significant tropospheric forcing of −33 ± 42 mWm^{-2}, with few models reporting positive forcings (Table 12 in Stevenson et al., 2013). The impact of climate change on ozone forcing is surrounded by large uncertainties, which are associated with chemistry-climate feedbacks and the lack of confidence in the LNO_x sensitivity to global mean surface temperature, due to different parameterizations and the vertical distributions of the emissions (Banerjee et al., 2014; Finney et al., 2016), as well as changes in the BDC (Butchart, 2014). For example, the climate change-induced net ozone forcing between 2000–2100 – following the future emission scenario RCP8.5 in an independent CCM – is of the same order of magnitude but different sign (−70 mWm^{-2}) (Banerjee et al., 2018). While they found similar

tropospheric ozone forcing of 70 mWm^{-2}, their negative stratospheric ozone forcing outweighs the latter (−150 mWm^{-2}). Methane- and ODSs-induced ozone forcings have respectively a substantial contribution from the stratosphere (~14 %) and the troposphere (~34 %), recently shown in modelling studies (Søvde et al., 2011; Shindell et al., 2013; Banerjee et al., 2018). A striking result, however, is the contribution of the stratospheric-produced ozone to the net forcing of ~30 ± 20 % and ~99 ± 50 % due to methane and ODS concentrations respectively, which is consistent with the findings from an independent chemistry-climate model (Banerjee et al., 2016, 2018). This reflects the roles that methane plays in stratospheric ozone chemistry (i.e. particularly in the lower stratosphere), and that ozone recovery principally occurs in the stratosphere.

5 Summary and conclusions

This study has explored future changes in ozone by the end of the 21st century and the resulting radiative forcing following a process-based approach, imposing one forcing at a time. We have used the RCP8.5 emissions scenario to represent an upper limit on these responses. This is a different approach to previous studies, which typically have either explored future changes in ozone concentrations or ozone forcing. The methane feedbacks (due to the changing oxidising capacity of the atmosphere, and due to the long-term tropospheric ozone response) and its forcing have also been accounted for. In addition, non-linearities arising from chemistry-climate interactions have been investigated.

The simulated present-day ozone radiative effect (RE) is in good agreement with estimates based on observed ozone from TES, particularly in terms of its spatial distribution. However, there are systematic biases: RE is overestimated in the NH and underestimated in the SH, with significant biases in the subtropics. These RE biases are mostly consistent with the biases in tropospheric ozone in current global chemistry-climate models (Young et al., 2018), although the simulated annual global present-day tropospheric column ozone (28.9 ± 1.5 DU) is within observed interannual variability of 28.1–34.1 DU (Young et al., 2013). The fact that similar spatial distribution biases are apparent in many climate models suggests a common

deficiency, and emissions data have been proposed as a likely candidate (Young et al., 2013; Young et al., 2018).

Our analysis shows that the net ozone radiative forcing arising from climate driven changes is relatively small and not significant (33 ± 104 mWm^{-2}), which is largely the result of the interplay between lightning-produced ozone and enhanced ozone destruction (via increased temperatures and humidity). Higher methane concentrations and reduced ODS levels also have consequences for ozone forcing in the stratosphere (45 ± 39 mWm^{-2}) and the troposphere (46 ± 47 mWm^{-2}) respectively. We have demonstrated both the importance of stratospheric-tropospheric interactions and the stratosphere as a key region controlling a large fraction of the tropospheric ozone forcing (i.e. from the source point of view compared to the more common division by recipient-region).

Future annual and global tropospheric and stratospheric column ozone changes from year 2000 to 2100 in this set of simulations (7.0 DU and 21.3 DU respectively) are mainly driven by methane and ODS emissions, respectively (Table S1). These changes lead to a net ozone radiative forcing of 430 ± 130 mWm^{-2} compared to present-day, with an overall uncertainty of ±30 % (i.e. representing the 95 % confidence interval). Relative to the pre-industrial period (year 1750), our best estimate for the year 2100 net ozone radiative forcing is 760 ± 230 mWm^{-2}.

This study highlights the key role of the stratosphere in determining future ozone radiative forcing in spite of the fact that the impacts largely take place in the troposphere. Increasing confidence in present-day observations of the Brewer-Dobson circulation and the stratospheric-tropospheric exchange will therefore play a crucial role in improving chemistry-climate models and better constraining ozone radiative forcing. A future study will address the importance of the stratosphere on future air quality commitments, which may better inform emission regulations.

Competing interests. The authors declare that they have no conflict of interest.

Data availability. The model output used here can be available upon request from the corresponding author (figlesias@iqfr.csic.es). The whole atmosphere ozone radiative kernel can also be available upon request from A. Rap (a.rap@leeds.ac.uk).

Acknowledgements. This work was supported by NERC, under project number NE/L501736/1. F. Iglesias-Suarez would like to acknowledge NERC for a PhD studentship and thank F. Govantes for hosting him at the Centro Andaluz de Biología del Desarrollo (CABD) while he completed some of this work. WACCM is a component of the Community Earth System Model (CESM), which is supported by the NSF and the Office of Science of the U.S. Department of Energy. Computing resources were provided by NCAR's Climate Simulation Laboratory, sponsored by the NSF and other agencies. This research was enabled by the computational and storage resources of NCAR's Computational and Information Systems Laboratory (CISL). We thank the NASA JPL TES team for releasing the TES ozone.

References

Andrews, D. G., Holton, J. R., and Leovy, C. B.: Middle atmosphere dynamics, International Geophysics Series, Academic press, San Diego, USA, 1987.

Arblaster et al.: Stratospheric ozone changes and climate, Chapter 4, in: Scientific Assessment of Ozone Depletion: 2014, Global Ozone Research and Monitoring Project, 2014.

Austin, J., and Wilson, R. J.: Ensemble simulations of the decline and recovery of stratospheric ozone, J. Geophys. Res., 111, 2156-2202, doi:10.1029/2005JD006907, 2006.

Avallone, L. M., and Prather, M. J.: Photochemical evolution of ozone in the lower tropical stratosphere, J. Geophys. Res., 101, 1457-1461, doi:10.1029/95JD03010, 1996.

Banerjee, A., Archibald, A. T., Maycock, A. C., Telford, P., Abraham, N. L., Yang, X., Braesicke, P., and Pyle, J. A.: Lightning NOx, a key chemistry–climate interaction: impacts of future climate change and consequences for tropospheric oxidising capacity, Atmos. Chem. Phys., 14, 9871-9881, doi:10.5194/acp-14-9871-2014, 2014.

Banerjee, A., Maycock, A. C., Archibald, A. T., Abraham, N. L., Telford, P., Braesicke, P., and Pyle, J. A.: Drivers of changes in stratospheric and tropospheric ozone between year 2000 and 2100, Atmos. Chem. Phys., 16, 2727-2746, doi:10.5194/acp-16-2727-2016, 2016.

Banerjee, A., Maycock, A. C., and Pyle, J. A.: Chemical and climatic drivers of radiative forcing due to changes in stratospheric and tropospheric ozone over the 21st century, Atmos. Chem. Phys., 18, 2899-2911, doi:10.5194/acp-18-2899-2018, 2018.

Bekki, S., A. Rap, V. Poulain, S. Dhomse, M. Marchand, F. Lefevre, P. M. Forster, S. Szopa, and M. P. Chipperfield (2013), Climate impact of stratospheric ozone recovery, Geophys. Res. Lett., 40, 2796–2800, doi:10.1002/grl.50358.

Berntsen, T. K., Isaksen, I. S. A., Myhre, G., Fuglestvedt, J. S., Stordal, F., Larsen, T. A., Freckleton, R. S., and Shine, K. P.: Effects of anthropogenic emissions on tropospheric ozone and its radiative forcing, J. Geophys. Res., 102, 2156-2202, doi:10.1029/97JD02226, 1997.

Birner, T., and Bönisch, H.: Residual circulation trajectories and transit times into the extratropical lowermost stratosphere, Atmos. Chem. Phys., 11, 817-827, doi:10.5194/acp-11-817-2011, 2011.

Brasseur, G. P., Schultz, M., Granier, C., Saunois, M., Diehl, T., Botzet, M., Roeckner, E., and Walters, S.: Impact of Climate Change on the Future Chemical Composition of the Global Troposphere, J. Clim., 19, 3932-3951, doi:10.1175/JCLI3832.1, 2006.

Butchart, N., Cionni, I., Eyring, V., Shepherd, T. G., Waugh, D. W., Akiyoshi, H., Austin, J., Brühl, C., Chipperfield, M. P., Cordero, E., Dameris, M., Deckert, R., Dhomse, S., Frith, S. M., Garcia, R. R., Gettelman, A., Giorgetta, M. A., Kinnison, D. E., Li, F., Mancini, E., McLandress, C., Pawson, S., Pitari, G., Plummer, D. A., Rozanov, E., Sassi, F., Scinocca, J. F., Shibata, K., Steil, B., and Tian, W.: Chemistry–Climate Model Simulations of Twenty-First Century Stratospheric

Climate and Circulation Changes, J. Clim., 23, 5349-5374, doi:10.1175/2010JCLI3404.1, 2010.

Butchart, N.: The Brewer-Dobson circulation, Rev. Geophys., 52, 157-184, doi:10.1002/2013RG000448, 2014.

Calvo, N., Garcia, R. R., and Kinnison, D. E.: Revisiting Southern Hemisphere polar stratospheric temperature trends in WACCM: The role of dynamical forcing, Geophys. Res. Lett., 44, 2017GL072792, doi:10.1002/2017GL072792, 2017.

Chipperfield, M. P., Bekki, S., Dhomse, S., Harris, N. R. P., Hassler, B., Hossaini, R., Steinbrecht, W., Thiéblemont, R., and Weber, M.: Detecting recovery of the stratospheric ozone layer, Nature, 549, 211-218, doi:10.1038/nature23681, 2017.

Collins, W. J., Derwent, R. G., Garnier, B., Johnson, C. E., Sanderson, M. G., and Stevenson, D. S.: Effect of stratosphere-troposphere exchange on the future tropospheric ozone trend, J. Geophys. Res., 108, 8528, doi:10.1029/2002JD002617, 2003.

Dahlmann, K., Grewe, V., Ponater, M., and Matthes, S.: Quantifying the contributions of individual NOx sources to the trend in ozone radiative forcing, Atmos. Environ., 45, 2860-2868, doi:10.1016/j.atmosenv.2011.02.071, 2011.

Edwards, J. M., and Slingo, A.: Studies with a flexible new radiation code. I: Choosing a configuration for a large-scale model, Quart. J. Roy. Meteor. Soc., 122, 689-719, doi:10.1002/qj.49712253107, 1996.

Emmons, L. K., Walters, S., Hess, P. G., Lamarque, J. F., Pfister, G. G., Fillmore, D., Granier, C., Guenther, A., Kinnison, D., Laepple, T., Orlando, J., Tie, X., Tyndall, G., Wiedinmyer, C., Baughcum, S. L., and Kloster, S.: Description and evaluation of the Model for Ozone and Related chemical Tracers, version 4 (MOZART-4), Geosci. Model Dev., 3, 43-67, doi:10.5194/gmd-3-43-2010, 2010.

Engel, A., Mobius, T., Bonisch, H., Schmidt, U., Heinz, R., Levin, I., Atlas, E., Aoki, S., Nakazawa, T., Sugawara, S., Moore, F., Hurst, D., Elkins, J., Schauffler, S., Andrews, A., and Boering, K.: Age of stratospheric air unchanged within uncertainties over the past 30 years, Nature Geosci., 2, 28-31, doi:10.1038/ngeo388, 2009.

Eyring, V., Cionni, I., Bodeker, G. E., Charlton-Perez, A. J., Kinnison, D. E., Scinocca, J. F., Waugh, D. W., Akiyoshi, H., Bekki, S., Chipperfield, M. P., Dameris, M., Dhomse, S., Frith, S. M., Garny, H., Gettelman, A., Kubin, A., Langematz, U., Mancini, E., Marchand, M., Nakamura, T., Oman, L. D., Pawson, S., Pitari, G., Plummer, D. A., Rozanov, E., Shepherd, T. G., Shibata, K., Tian, W., Braesicke, P., Hardiman, S. C., Lamarque, J. F., Morgenstern, O., Pyle, J. A., Smale, D., and Yamashita, Y.: Multi-model assessment of stratospheric ozone return dates and ozone recovery in CCMVal-2 models, Atmos. Chem. Phys., 10, 9451-9472, doi:10.5194/acp-10-9451-2010, 2010.

Eyring, V., Lamarque, J.-F., Hess, P., Arfeuille, F., Bowman, K., Chipperfield, M. P., Duncan, B., Fiore, A., Gettelman, A., Giorgetta, M. a., Granier, C., Hegglin, M. I., Kinnison, D., Kunze, M., Langematz, U., Luo, B., Martin, R., Matthes, K., Newman, P. a., Peter, T., Robock, A., Ryerson, T., Saiz-Lopez, A., Salawitch, R., Schultz, M., Shepherd, T. G., Shindell, D., Stähelin, J., Tegtmeier, S., Thomason, L., Tilmes, S., Vernier, J.-P., Waugh, D. W., and Young, P. J.: Overview of IGAC/SPARC Chemistry-Climate Model Initiative (CCMI) Community Simulations in Support of

Upcoming Ozone and Climate Assessments, WMO-WRCP, Geneva, Switzerland, 48-66, 2013.

Fels, S. B., Mahlman, J. D., Schwarzkopf, M. D., and Sinclair, R. W.: Stratospheric Sensitivity to Perturbations in Ozone and Carbon Dioxide: Radiative and Dynamical Response, J. Atmos. Sci., 37, 2265-2297, doi:10.1175/1520-0469(1980)037<2265:sstpio>2.0.co;2, 1980.

Finney, D. L., Doherty, R. M., Wild, O., Young, P. J., and Butler, A.: Response of lightning NOx emissions and ozone production to climate change: Insights from the Atmospheric Chemistry and Climate Model Intercomparison Project, Geophys. Res. Lett., 43, 2016GL068825, doi:10.1002/2016GL068825, 2016.

Fiore, A. M., Dentener, F. J., Wild, O., Cuvelier, C., Schultz, M. G., Hess, P., Textor, C., Schulz, M., Doherty, R. M., Horowitz, L. W., MacKenzie, I. A., Sanderson, M. G., Shindell, D. T., Stevenson, D. S., Szopa, S., Van Dingenen, R., Zeng, G., Atherton, C., Bergmann, D., Bey, I., Carmichael, G., Collins, W. J., Duncan, B. N., Faluvegi, G., Folberth, G., Gauss, M., Gong, S., Hauglustaine, D., Holloway, T., Isaksen, I. S. A., Jacob, D. J., Jonson, J. E., Kaminski, J. W., Keating, T. J., Lupu, A., Marmer, E., Montanaro, V., Park, R. J., Pitari, G., Pringle, K. J., Pyle, J. A., Schroeder, S., Vivanco, M. G., Wind, P., Wojcik, G., Wu, S., and Zuber, A.: Multimodel estimates of intercontinental source-receptor relationships for ozone pollution, J. Geophys. Res., 114, D04301, doi:10.1029/2008JD010816, 2009.

Fleming, E. L., Jackman, C. H., Stolarski, R. S., and Douglass, A. R.: A model study of the impact of source gas changes on the stratosphere for 1850–2100, Atmos. Chem. Phys., 11, 8515-8541, doi:10.5194/acp-11-8515-2011, 2011.

Forster, P. M., and Shine, K. P.: Radiative forcing and temperature trends from stratospheric ozone changes, J. Geophys. Res., 102, 10841-10855, doi:10.1029/96JD03510, 1997.

Fuglestvedt, J. S., Berntsen, T. K., Isaksen, I. S. A., Mao, H., Liang, X.-Z., and Wang, W.-C.: Climatic forcing of nitrogen oxides through changes in tropospheric ozone and methane; global 3D model studies, Atmos. Environ., 33, 961-977, doi:10.1016/S1352-2310(98)00217-9, 1999.

Galloway, J. N., Dentener, F. J., Capone, D. G., Boyer, E. W., Howarth, R. W., Seitzinger, S. P., Asner, G. P., Cleveland, C. C., Green, P. A., Holland, E. A., Karl, D. M., Michaels, A. F., Porter, J. H., Townsend, A. R., and Vöosmarty, C. J.: Nitrogen Cycles: Past, Present, and Future, Biogeochemistry, 70, 153-226, doi:10.1007/s10533-004-0370-0, 2004.

Garcia, R. R., and Randel, W. J.: Acceleration of the Brewer–Dobson Circulation due to Increases in Greenhouse Gases, J. Atmos. Sci., 65, 2731-2739, doi:10.1175/2008JAS2712.1, 2008.

Garcia, R. R., Smith, A. K., Kinnison, D. E., Cámara, Á. d. l., and Murphy, D. J.: Modification of the Gravity Wave Parameterization in the Whole Atmosphere Community Climate Model: Motivation and Results, J. Atmos. Sci., 74, 275-291, doi:10.1175/JAS-D-16-0104.1, 2017.

Gauss, M., Myhre, G., Pitari, G., Prather, M. J., Isaksen, I. S. A., Berntsen, T. K., Brasseur, G. P., Dentener, F. J., Derwent, R. G., Hauglustaine, D. A., Horowitz, L. W., Jacob, D. J., Johnson, M., Law, K. S., Mickley, L. J., Müller, J. F., Plantevin, P. H., Pyle, J. A., Rogers, H. L., Stevenson, D. S., Sundet, J. K., van Weele, M., and

Wild, O.: Radiative forcing in the 21st century due to ozone changes in the troposphere and the lower stratosphere, J. Geophys. Res., 108, 4292, doi:10.1029/2002JD002624, 2003.

Guenther, A. B., Jiang, X., Heald, C. L., Sakulyanontvittaya, T., Duhl, T., Emmons, L. K., and Wang, X.: The Model of Emissions of Gases and Aerosols from Nature version 2.1 (MEGAN2.1): an extended and updated framework for modeling biogenic emissions, Geosci. Model Dev., 5, 1471-1492, doi:10.5194/gmd-5-1471-2012, 2012.

Haigh, J. D., and Pyle, J. A.: Ozone perturbation experiments in a two-dimensional circulation model, Quart. J. Roy. Meteor. Soc., 108, 551-574, doi:10.1002/qj.49710845705, 1982.

Hardiman, S. C., Butchart, N., and Calvo, N.: The morphology of the Brewer–Dobson circulation and its response to climate change in CMIP5 simulations, Quart. J. Roy. Meteor. Soc., 140, 1958-1965, doi:10.1002/qj.2258, 2014.

Hegglin, M. I., and Shepherd, T. G.: Large climate-induced changes in ultraviolet index and stratosphere-to-troposphere ozone flux, Nature Geosci., 2, 687-691, doi:10.1038/ngeo604, 2009.

Hegglin, M. I., Plummer, D. A., Shepherd, T. G., Scinocca, J. F., Anderson, J., Froidevaux, L., Funke, B., Hurst, D., Rozanov, A., Urban, J., von Clarmann, T., Walker, K. A., Wang, H. J., Tegtmeier, S., and Weigel, K.: Vertical structure of stratospheric water vapour trends derived from merged satellite data, Nature Geosci., 7, 768-776, doi:10.1038/ngeo2236, 2014.

Holmes, C. D., Prather, M. J., Søvde, O. A., and Myhre, G.: Future methane, hydroxyl, and their uncertainties: key climate and emission parameters for future predictions, Atmos. Chem. Phys., 13, 285-302, doi:10.5194/acp-13-285-2013, 2013.

Iglesias-Suarez, F., Young, P. J., and Wild, O.: Stratospheric ozone change and related climate impacts over 1850–2100 as modelled by the ACCMIP ensemble, Atmos. Chem. Phys., 16, 343-363, doi:10.5194/acp-16-343-2016, 2016.

Jacob, D.: Introduction to atmospheric chemistry, Princeton University Press, Princeton, USA, 1999.

Johnson, C. E., Stevenson, D. S., Collins, W. J., and Derwent, R. G.: Role of climate feedback on methane and ozone studied with a Coupled Ocean-Atmosphere-Chemistry Model, Geophys. Res. Lett., 28, 1723-1726, doi:10.1029/2000GL011996, 2001.

Kawase, H., Nagashima, T., Sudo, K., and Nozawa, T.: Future changes in tropospheric ozone under Representative Concentration Pathways (RCPs), Geophys. Res. Lett., 38, 1944-8007, doi:10.1029/2010gl046402, 2011.

Kinnison, D. E., Brasseur, G. P., Walters, S., Garcia, R. R., Marsh, D. R., Sassi, F., Harvey, V. L., Randall, C. E., Emmons, L., Lamarque, J. F., Hess, P., Orlando, J. J., Tie, X. X., Randel, W., Pan, L. L., Gettelman, A., Granier, C., Diehl, T., Niemeier, U., and Simmons, A. J.: Sensitivity of chemical tracers to meteorological parameters in the MOZART-3 chemical transport model, J. Geophys. Res., 112, 2156-2202, doi:10.1029/2006JD007879, 2007.

Lacis, A. A., Wuebbles, D. J., and Logan, J. A.: Radiative forcing of climate by changes in the vertical distribution of ozone, J. Geophys. Res., 95, 9971-9981, doi:10.1029/JD095iD07p09971, 1990.

Lamarque, J. F., Emmons, L. K., Hess, P. G., Kinnison, D. E., Tilmes, S., Vitt, F., Heald, C. L., Holland, E. A., Lauritzen, P. H., Neu, J., Orlando, J. J., Rasch, P. J., and Tyndall, G. K.: CAM-chem: description and evaluation of interactive atmospheric chemistry in the Community Earth System Model, Geosci. Model Dev., 5, 369-411, doi:10.5194/gmd-5-369-2012, 2012.

Liaskos, C. E., Allen, D. J., and Pickering, K. E.: Sensitivity of tropical tropospheric composition to lightning NOx production as determined by replay simulations with GEOS-5, J. Geophys. Res., 120, 2014JD022987, doi:10.1002/2014JD022987, 2015.

Marsh, D. R., Mills, M. J., Kinnison, D. E., Lamarque, J.-F., Calvo, N., and Polvani, L. M.: Climate Change from 1850 to 2005 Simulated in CESM1(WACCM), J. Clim., 26, 7372-7391, doi:10.1175/JCLI-D-12-00558.1, 2013.

Meinshausen, M., Smith, S. J., Calvin, K., Daniel, J. S., Kainuma, M. L. T., Lamarque, J. F., Matsumoto, K., Montzka, S. A., Raper, S. C. B., Riahi, K., Thomson, A., Velders, G. J. M., and Vuuren, D. P. P.: The RCP greenhouse gas concentrations and their extensions from 1765 to 2300, Clim. Change, 109, 213-241, doi:10.1007/s10584-011-0156-z, 2011.

Morgenstern, O., Zeng, G., Luke Abraham, N., Telford, P. J., Braesicke, P., Pyle, J. A., Hardiman, S. C., O'Connor, F. M., and Johnson, C. E.: Impacts of climate change, ozone recovery, and increasing methane on surface ozone and the tropospheric oxidizing capacity, J. Geophys. Res., 118, 1028-1041, doi:10.1029/2012JD018382, 2013.

Morgenstern, O., Hegglin, M. I., Rozanov, E., O'Connor, F. M., Abraham, N. L., Akiyoshi, H., Archibald, A. T., Bekki, S., Butchart, N., Chipperfield, M. P., Deushi, M., Dhomse, S. S., Garcia, R. R., Hardiman, S. C., Horowitz, L. W., Jöckel, P., Josse, B., Kinnison, D., Lin, M., Mancini, E., Manyin, M. E., Marchand, M., Marécal, V., Michou, M., Oman, L. D., Pitari, G., Plummer, D. A., Revell, L. E., Saint-Martin, D., Schofield, R., Stenke, A., Stone, K., Sudo, K., Tanaka, T. Y., Tilmes, S., Yamashita, Y., Yoshida, K., and Zeng, G.: Review of the global models used within phase 1 of the Chemistry–Climate Model Initiative (CCMI), Geosci. Model Dev., 10, 639-671, doi:10.5194/gmd-10-639-2017, 2017.

Myhre, G., Shindell, D., Breìon, F.-M., Collins, W., Fuglestvedt, J., Huang, J., Koch, D., Lamarque, J.-F., Lee, D., Mendoza, B., Nakajima, T., Robock, A., Stephens, G., Takemura, T., and Zhang, H.: Anthropogenic and Natural Radiative Forcing, in: Climate Change: The Physical Science Basis. Contribution of Working Group I to the Fifth Assessment Report of the Intergovernmental Panel on Climate Change, [Stocker, T. F., Qin, D., Plattner, G.-K., Tignor, M., Allen, S. K., Boschung, J., Nauels, A., Xia, Y., Bex, V., and Midgley, P. M. (eds)], Cambridge University Press, Cambridge, United Kingdom and New York, NY, USA, 659–740, 2013.

Oberländer, S., Langematz, U., and Meul, S.: Unraveling impact factors for future changes in the Brewer-Dobson circulation, J. Geophys. Res., 118, 10,296-210,312, doi:10.1002/jgrd.50775, 2013.

Osterman, G. B., Kulawik, S. S., Worden, H. M., Richards, N. A. D., Fisher, B. M., Eldering, A., Shephard, M. W., Froidevaux, L., Labow, G., Luo, M., Herman, R. L., Bowman, K. W., and Thompson, A. M.: Validation of Tropospheric Emission Spectrometer (TES) measurements of the total, stratospheric, and tropospheric column abundance of ozone, J. Geophys. Res., 113, D15S16, doi:10.1029/2007JD008801, 2008.

Ploeger, F., Riese, M., Haenel, F., Konopka, P., Müller, R., and Stiller, G.: Variability of stratospheric mean age of air and of the local effects of residual circulation and eddy mixing, J. Geophys. Res., 120, 2014JD022468, 10.1002/2014JD022468, 2015.

Portmann, R. W., and Solomon, S.: Indirect radiative forcing of the ozone layer during the 21st century, Geophys. Res. Lett., 34, L02813, doi:10.1029/2006GL028252, 2007.

Prather M., Ehhalt, D., Dentener, F., Derwent, R., Dlugokencky, E., Holland, E., Isaksen, I., Katima, J., Kirchhoff, V., Matson, P., Midgley, P., Wang, M., Atmospheric chemistry and greenhouse gases. In: Climate change: The scientific basis. Contribution of Working Group I to the Third Assessment Report of the Intergovernmental Panel on Climate Change, [Houghton J. T., Ding, Y., Griggs, D. J., Noguer, M., van der Linden, P. J., Dai, X., Maskell, K., Johnson, C. A. (eds)], Cambridge University Press, Cambridge, UK, 2001.

Prather, M. J., Zhu, X., Tang, Q., Hsu, J., and Neu, J. L.: An atmospheric chemist in search of the tropopause, J. Geophys. Res., 116, 2156-2202, doi:10.1029/2010JD014939, 2011.

Prather, M. J., Holmes, C. D., and Hsu, J.: Reactive greenhouse gas scenarios: Systematic exploration of uncertainties and the role of atmospheric chemistry, Geophys. Res. Lett., 39, L09803, doi:10.1029/2012GL051440, 2012.

Price, J. D., and Vaughan, G.: The potential for stratosphere-troposphere exchange in cut-off-low systems, Quart. J. Roy. Meteor. Soc., 119, 343-365, doi:10.1002/qj.49711951007, 1993.

Randeniya, L. K., Vohralik, P. F., and Plumb, I. C.: Stratospheric ozone depletion at northern mid latitudes in the 21st century: The importance of future concentrations of greenhouse gases nitrous oxide and methane, Geophys. Res. Lett., 29, 10-11-10-14, doi:10.1029/2001GL014295, 2002.

Rap, A., Richards, N. A. D., Forster, P. M., Monks, S. A., Arnold, S. R., and Chipperfield, M. P.: Satellite constraint on the tropospheric ozone radiative effect, Geophys. Res. Lett., 42, 2015GL064037, doi:10.1002/2015GL064037, 2015.

Ray, E. A., Moore, F. L., Rosenlof, K. H., Davis, S. M., Sweeney, C., Tans, P., Wang, T., Elkins, J. W., Bönisch, H., Engel, A., Sugawara, S., Nakazawa, T., and Aoki, S.: Improving stratospheric transport trend analysis based on SF6 and CO2 measurements, J. Geophys. Res., 119, 2014JD021802, doi:10.1002/2014JD021802, 2014.

Revell, L. E., Bodeker, G. E., Smale, D., Lehmann, R., Huck, P. E., Williamson, B. E., Rozanov, E., and Struthers, H.: The effectiveness of N2O in depleting stratospheric ozone, Geophys. Res. Lett., 39, L15806, doi:10.1029/2012GL052143, 2012.

Riese, M., Ploeger, F., Rap, A., Vogel, B., Konopka, P., Dameris, M., and Forster, P.: Impact of uncertainties in atmospheric mixing on simulated UTLS composition and related radiative effects, J. Geophys. Res., 117, D16305, doi:10.1029/2012JD017751, 2012.

Roelofs, G.-J., and Lelieveld, J.: Model study of the influence of cross-tropopause O3 transports on tropospheric O3 levels, Tellus, Ser. B, 49, 38-55, doi:10.3402/tellusb.v49i1.15949, 1997.

Rosenfield, J. E., Douglass, A. R., and Considine, D. B.: The impact of increasing carbon dioxide on ozone recovery, J. Geophys. Res., 107, ACH 7-1-ACH 7-9, doi:10.1029/2001JD000824, 2002.

Rossow, W. B., and Schiffer, R. A.: Advances in Understanding Clouds from ISCCP, Bull. Am. Meteorol. Soc., 80, 2261-2288, doi:10.1175/1520-0477(1999)080<2261:aiucfi>2.0.co;2, 1999.

Schumann, U., and Huntrieser, H.: The global lightning-induced nitrogen oxides source, Atmos. Chem. Phys., 7, 3823-3907, doi:10.5194/acp-7-3823-2007, 2007.

Shindell, D., Faluvegi, G., Nazarenko, L., Bowman, K., Lamarque, J. F., Voulgarakis, A., Schmidt, G. A., Pechony, O., and Ruedy, R.: Attribution of historical ozone forcing to anthropogenic emissions, Nature Clim. Change, 3, 567-570, doi:10.1038/nclimate1835, 2013.

Sillman, S.: The relation between ozone, NOx and hydrocarbons in urban and polluted rural environments, Atmos. Environ., 33, 1821-1845, doi:10.1016/S1352-2310(98)00345-8, 1999.

Skeie, R. B., Berntsen, T. K., Myhre, G., Tanaka, K., Kvalevåg, M. M., and Hoyle, C. R.: Anthropogenic radiative forcing time series from pre-industrial times until 2010, Atmos. Chem. Phys., 11, 11827-11857, doi:10.5194/acp-11-11827-2011, 2011.

Solomon, S., Kinnison, D., Bandoro, J., and Garcia, R.: Simulation of polar ozone depletion: An update, J. Geophys. Res., 120, 2015JD023365, doi:10.1002/2015JD023365, 2015.

Søvde, O. A., Hoyle, C. R., Myhre, G., and Isaksen, I. S. A.: The HNO3 forming branch of the HO2 + NO reaction: pre-industrial-to-present trends in atmospheric species and radiative forcings, Atmos. Chem. Phys., 11, 8929-8943, doi:10.5194/acp-11-8929-2011, 2011.

Squire, O. J., Archibald, A. T., Abraham, N. L., Beerling, D. J., Hewitt, C. N., Lathière, J., Pike, R. C., Telford, P. J., and Pyle, J. A.: Influence of future climate and cropland expansion on isoprene emissions and tropospheric ozone, Atmos. Chem. Phys., 14, 1011-1024, doi:10.5194/acp-14-1011-2014, 2014.

Stenke, A., and Grewe, V.: Simulation of stratospheric water vapor trends: impact on stratospheric ozone chemistry, Atmos. Chem. Phys., 5, 1257-1272, doi:10.5194/acp-5-1257-2005, 2005.

Stevenson, D. S., Dentener, F. J., Schultz, M. G., Ellingsen, K., van Noije, T. P. C., Wild, O., Zeng, G., Amann, M., Atherton, C. S., Bell, N., Bergmann, D. J., Bey, I., Butler, T., Cofala, J., Collins, W. J., Derwent, R. G., Doherty, R. M., Drevet, J., Eskes, H. J., Fiore, A. M., Gauss, M., Hauglustaine, D. A., Horowitz, L. W., Isaksen, I. S. A., Krol, M. C., Lamarque, J. F., Lawrence, M. G., Montanaro, V., Müller, J. F., Pitari, G., Prather, M. J., Pyle, J. A., Rast, S., Rodriguez, J. M., Sanderson, M. G., Savage, N. H., Shindell, D. T., Strahan, S. E., Sudo, K., and Szopa, S.: Multimodel ensemble simulations of present-day and near-future tropospheric ozone, J. Geophys. Res., 111, D08301, doi:10.1029/2005JD006338, 2006.

Stevenson, D. S., Young, P. J., Naik, V., Lamarque, J. F., Shindell, D. T., Voulgarakis, A., Skeie, R. B., Dalsoren, S. B., Myhre, G., Berntsen, T. K., Folberth, G. A., Rumbold, S. T., Collins, W. J., MacKenzie, I. A., Doherty, R. M., Zeng, G., van Noije, T. P. C., Strunk, A., Bergmann, D., Cameron-Smith, P., Plummer, D. A.,

Strode, S. A., Horowitz, L., Lee, Y. H., Szopa, S., Sudo, K., Nagashima, T., Josse, B., Cionni, I., Righi, M., Eyring, V., Conley, A., Bowman, K. W., Wild, O., and Archibald, A.: Tropospheric ozone changes, radiative forcing and attribution to emissions in the Atmospheric Chemistry and Climate Model Intercomparison Project (ACCMIP), Atmos. Chem. Phys., 13, 3063-3085, doi:10.5194/acp-13-3063-2013, 2013.

Stiller, G. P., Fierli, F., Ploeger, F., Cagnazzo, C., Funke, B., Haenel, F. J., Reddmann, T., Riese, M., and von Clarmann, T.: Shift of subtropical transport barriers explains observed hemispheric asymmetry of decadal trends of age of air, Atmos. Chem. Phys., 17, 11177-11192, doi:10.5194/acp-17-11177-2017, 2017.

Sudo, K., Takahashi, M., and Akimoto, H.: Future changes in stratosphere-troposphere exchange and their impacts on future tropospheric ozone simulations, Geophys. Res. Lett., 30, 2256, doi:10.1029/2003GL018526, 2003.

Tilmes, S., Lamarque, J. F., Emmons, L. K., Kinnison, D. E., Ma, P. L., Liu, X., Ghan, S., Bardeen, C., Arnold, S., Deeter, M., Vitt, F., Ryerson, T., Elkins, J. W., Moore, F., Spackman, J. R., and Val Martin, M.: Description and evaluation of tropospheric chemistry and aerosols in the Community Earth System Model (CESM1.2), Geosci. Model Dev., 8, 1395-1426, doi:10.5194/gmd-8-1395-2015, 2015.

Tilmes, S., Lamarque, J. F., Emmons, L. K., Kinnison, D. E., Marsh, D., Garcia, R. R., Smith, A. K., Neely, R. R., Conley, A., Vitt, F., Val Martin, M., Tanimoto, H., Simpson, I., Blake, D. R., and Blake, N.: Representation of the Community Earth System Model (CESM1) CAM4-chem within the Chemistry-Climate Model Initiative (CCMI), Geosci. Model Dev., 9, 1853-1890, doi:10.5194/gmd-9-1853-2016, 2016.

UNEP: Environmental effects of ozone depletion and its interaction with climate change: 2014 assessment, United Nations Environment Programme (UNEP), Nairobi, 2015.

Val Martin, M., Heald, C. L., and Arnold, S. R.: Coupling dry deposition to vegetation phenology in the Community Earth System Model: Implications for the simulation of surface O3, Geophys. Res. Lett., 41, 2988-2996, doi:10.1002/2014GL059651, 2014.

van Vuuren, Detlef, P., Edmonds, J., Kainuma, M., Riahi, K., Thomson, A., Hibbard, K., Hurtt, G., Kram, T., Krey, V., Lamarque, J.-F., Masui, T., Meinshausen, M., Nakicenovic, N., Smith, S., and Rose, S.: The representative concentration pathways: an overview, Clim. Change, 109, 5-31, doi:10.1007/s10584-011-0148-z, 2011.

Voulgarakis, A., Naik, V., Lamarque, J. F., Shindell, D. T., Young, P. J., Prather, M. J., Wild, O., Field, R. D., Bergmann, D., Cameron-Smith, P., Cionni, I., Collins, W. J., Dalsören, S. B., Doherty, R. M., Eyring, V., Faluvegi, G., Folberth, G. A., Horowitz, L. W., Josse, B., MacKenzie, I. A., Nagashima, T., Plummer, D. A., Righi, M., Rumbold, S. T., Stevenson, D. S., Strode, S. A., Sudo, K., Szopa, S., and Zeng, G.: Analysis of present day and future OH and methane lifetime in the ACCMIP simulations, Atmos. Chem. Phys., 13, 2563-2587, doi:10.5194/acp-13-2563-2013, 2013.

Wegner, T., Kinnison, D. E., Garcia, R. R., and Solomon, S.: Simulation of polar stratospheric clouds in the specified dynamics version of the whole atmosphere

community climate model, J. Geophys. Res., 118, 4991-5002, doi:10.1002/jgrd.50415, 2013.

Wilcox, L. J., Charlton-Perez, A. J., and Gray, L. J.: Trends in Austral jet position in ensembles of high- and low-top CMIP5 models, J. Geophys. Res., 117, D13115, doi:10.1029/2012JD017597, 2012.

Wild, O., and Prather, M. J.: Excitation of the primary tropospheric chemical mode in a global three-dimensional model, J. Geophys. Res., 105, 24647-24660, doi:10.1029/2000JD900399, 2000.

Wild, O.: Modelling the global tropospheric ozone budget: exploring the variability in current models, Atmos. Chem. Phys., 7, 2643-2660, doi:10.5194/acp-7-2643-2007, 2007.

Williams, E. R.: Lightning and climate: A review, Atmospheric Research, 76, 272-287, doi:10.1016/j.atmosres.2004.11.014, 2005.

WMO: Scientific Assessment of Ozone Depletion: 2010, World Meteorological Organization, Geneva, Switzerland, 516 pp., 2011.

WMO: Scientific Assessment of Ozone Depletion: 2014, World Meteorological Organization, Global Ozone Research and Monitoring Project, Geneva, Switzerland, 2014.

Worden, H. M., Bowman, K. W., Kulawik, S. S., and Aghedo, A. M.: Sensitivity of outgoing longwave radiative flux to the global vertical distribution of ozone characterized by instantaneous radiative kernels from Aura-TES, J. Geophys. Res., 116, D14115, doi:10.1029/2010JD015101, 2011.

Young, P. J., Archibald, A. T., Bowman, K. W., Lamarque, J. F., Naik, V., Stevenson, D. S., Tilmes, S., Voulgarakis, A., Wild, O., Bergmann, D., Cameron-Smith, P., Cionni, I., Collins, W. J., Dalsoren, S. B., Doherty, R. M., Eyring, V., Faluvegi, G., Horowitz, L. W., Josse, B., Lee, Y. H., MacKenzie, I. A., Nagashima, T., Plummer, D. A., Righi, M., Rumbold, S. T., Skeie, R. B., Shindell, D. T., Strode, S. A., Sudo, K., Szopa, S., and Zeng, G.: Pre-industrial to end 21st century projections of tropospheric ozone from the Atmospheric Chemistry and Climate Model Intercomparison Project (ACCMIP), Atmos. Chem. Phys., 13, 2063-2090, doi:10.5194/acp-13-2063-2013, 2013.

Young, P. J., Naik, V., Fiore, A. M., Gaudel, A., Guo, J., Lin, M. Y., Neu, J., Parrish, D. D., Rieder, H. E., Schnell, J. L., Tilmes, S., Wild, O., Zhang, L., Ziemke, J., Brandt, J., Delcloo, A., Doherty, R. M., Geels, C., Hegglin, M. I., Hu, L., Im, U., Kumar, R., Luhar, A., Murray, L., Plummer, D., Rodriguez, J., Saiz-Lopez, A., Schultz, M. G., Woodhouse, M., and Zeng, G., Tropospheric Ozone Assessment Report: Assessment of global-scale model performance for global and regional ozone distributions, variability, and trends, Elementa Science of the Anthropocene, 6, 10, doi: 10.1525/elementa.265, 2018.

Zeng, G., and Pyle, J. A.: Changes in tropospheric ozone between 2000 and 2100 modeled in a chemistry-climate model, Geophys. Res. Lett., 30, 1392, doi:10.1029/2002GL016708, 2003.

Zeng, G., Pyle, J. A., and Young, P. J.: Impact of climate change on tropospheric ozone and its global budgets, Atmos. Chem. Phys., 8, 369-387, doi:10.5194/acp-8-369-2008, 2008.

Zeng, G., Morgenstern, O., Braesicke, P., and Pyle, J. A.: Impact of stratospheric ozone recovery on tropospheric ozone and its budget, Geophys. Res. Lett., 37, L09805, doi:10.1029/2010GL042812, 2010.

Zhang, H., Wu, S., Huang, Y., and Wang, Y.: Effects of stratospheric ozone recovery on photochemistry and ozone air quality in the troposphere, Atmos. Chem. Phys., 14, 4079-4086, doi:10.5194/acp-14-4079-2014, 2014.

Table 1. Summary of the model simulations

Simulation	Climate[1]	ODSs[2]	CH_4[3]
Cnt	2000	2000	2000
Clm	2100 (fLNOx)[4]	2000	2000
Ltn	2100	2000	2000
O3r	2100	2100	2000
Mth	2100	2100	2100
Cnt+fLNOx	2000 (fLNOx)[4]	2000	2000

[1]Climate (SSTs, sea ice, CO_2 and N_2O, if not otherwise specified) follows the RCP8.5 emissions scenario.

[2]Relative to Cnt, ODS boundary conditions of −63.2 % (2.156 ppb) total chlorine, −35.7 % (8.1 ppt) total bromine and −67.6 % (1.376 ppb) total fluorine follow the halogen scenario A1.

[3]Relative to Cnt, CH_4 boundary conditions of 214.2 % (3744 ppb) follow the RCP8.5 emissions scenario.

[4]Offline lightning-induced NOx emissions are imposed by applying a monthly mean climatology of the Cnt simulation.

Table 2. Tropospheric ozone budget, including: Ozone production (P) and loss (L) terms are based on the gas-phase reaction rates of the O_x family (O_3, O, O^1D and NO_2); Net chemical production of ozone is defined as the residual of the production and loss terms (N = P − L); Dry deposition of ozone (D) term; Stratospheric-Tropospheric exchange (S; i.e. influx from the stratosphere) term is the residual of the dry deposition and net chemistry production terms (S = D − N); Ozone burden (B) term; Ozone and methane lifetimes (τ_{O3}, τ_{CH4} respectively) is the ratio between the burden and total losses (τ = burden / total loss); τ_{CH4} includes loss with respect to OH and adjusted for soil uptake (160 years) and stratospheric sink (120 years) (Prather et al., 2012); Burden for the stratospheric ozone tracer (B_{O3S}).

Simulation	P (Tg yr^{-1})	L (Tg yr^{-1})	N (Tg yr^{-1})	D (Tg yr^{-1})	S (Tg yr^{-1})	B (Tg)	τ_{O3} (years)	τ_{CH4} (years)	B_{O3S} (Tg)
ACCENT (year 2000)	5110 ± 606	4668 ± 727	442 ± 309	1003 ± 200	552 ± 168	344 ± 39	22.3 ± 2.0	8.7 ± 1.3	----
ACCMIP (year 2000)	4877 ± 853	4260 ± 645	618 ± 275	1094 ± 264	477 ± 97	337 ± 23	23.4 ± 2.2	8.5 ± 1.1	----
Cnt	4678	4195	483	881	398	318	22.9	7.2	123
Clm[1]	5111	4809	302	811	510	309	20.1	6.9	119
Ltn	5378	5057	322	833	511	329	20.4	6.6	138
O3r	5303	5058	245	855	610	337	20.8	6.6	131
Mth	6072	5759	313	979	666	378	20.5	8.3	138
Cnt+fLNOx[1]	4648	4169	479	878	399	313	22.7	7.2	121

[1] Offline lightning-induced NO_x emissions imposed by applying a monthly mean climatology of the Cnt simulation.

Table 3. Global and annual mean ozone RF and the standard error[a] (mWm^{-2}) by driver and region for the 2000–2100 period.

		Region		Source		CH_4[b]
	Whole-atmosphere	Tropo.	Strat.	Tropo.	Strat.	Tropo.
Climate (Clm−Cnt)[c]	−70 ± 102	−40 ± 42	−30 ± 35	−20 ± 21	−50 ± 57	−8
Lightning (Ltn−Clm)[c]	104 ± 108	105 ± 45	1 ± 37	79 ± 34	24 ± 48	−11
O3-recovery (O3r−Ltn)[d]	163 ± 109	46 ± 47	117 ± 38	1 ± 1	163 ± 84	2
Methane (Mth−O3r)[c]	238 ± 113	193 ± 51	45 ± 39	160 ± 42	78 ± 48	63
Total	435 ± 108	303 ± 48	132 ± 37	220 ± 13	214 ± 72	46

[a] The annual global mean is given along with the (±) standard error (i.e. associated with 10-year interannual variability of ozone).

[b] Long-term ozone forcing due to methane chemistry-climate feedback.

[c,d] RCP8.5 and halogen A1 emission scenarios by 2100 compared to year 2000 (Cnt run) respectively.

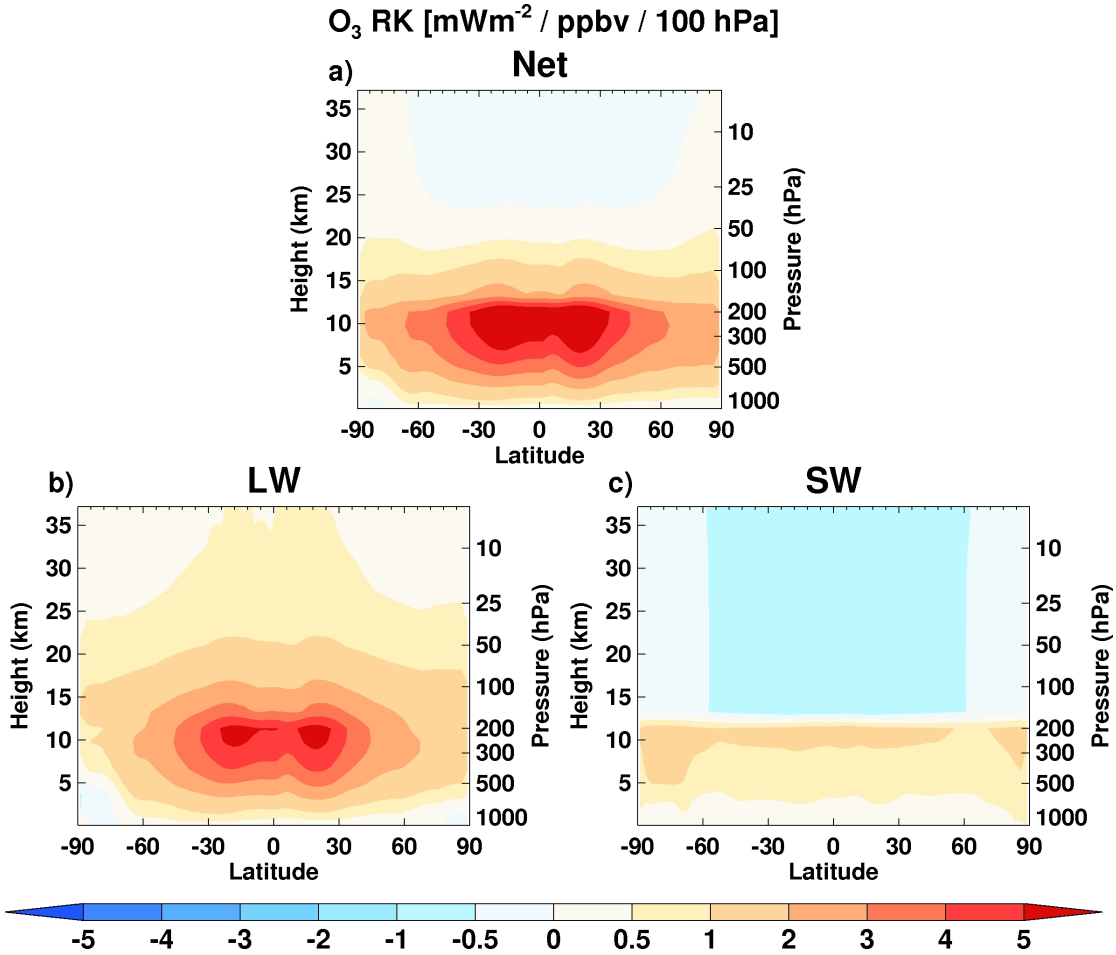

Figure 1. Annual zonal mean whole-atmosphere ozone radiative kernel under all-sky conditions for (a) net (LW+SW), (b) LW, and (c) SW components.

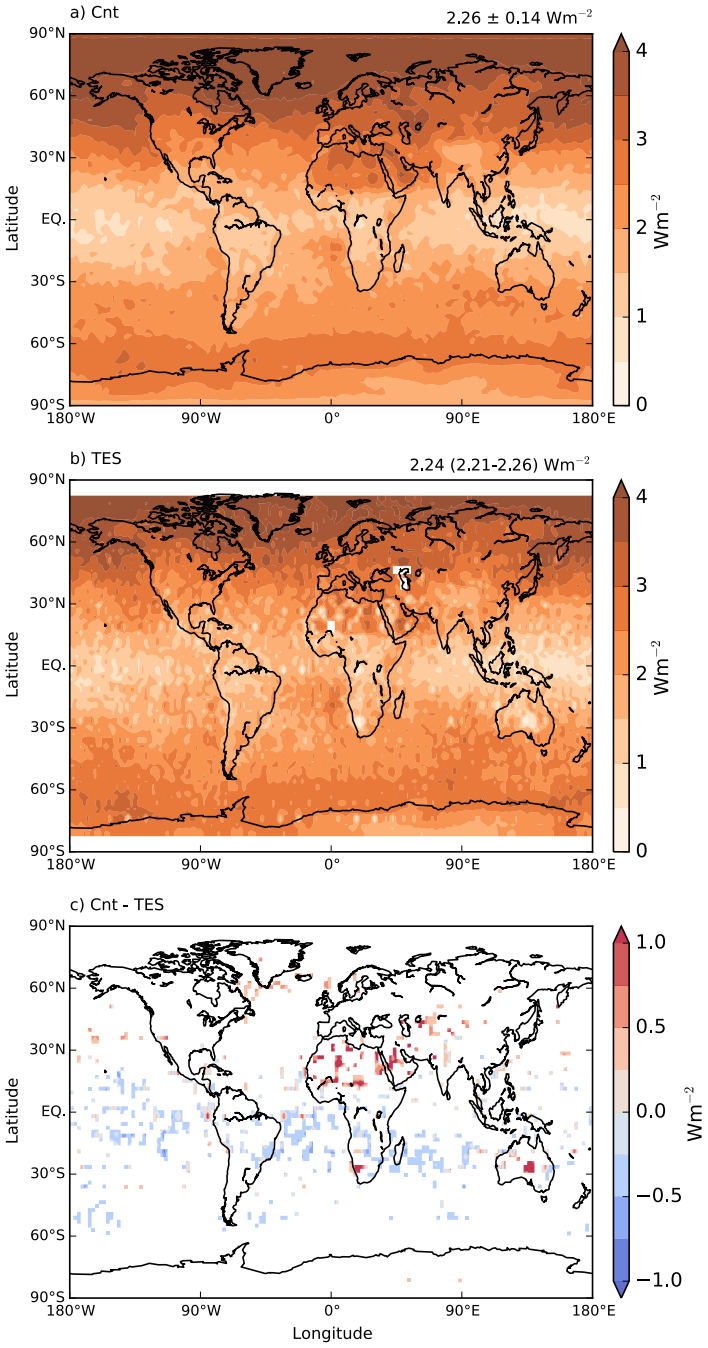

Figure 2. Comparison of the annual mean ozone radiative effect between (a) the Cnt simulation and (b) the Tropospheric Emission Spectrometer (TES) from July 2005 until June 2008 (05–08). (c) Cnt simulation bias compared to the TES. Differences are masked for the ±1.96 standard error within the three years observed range.

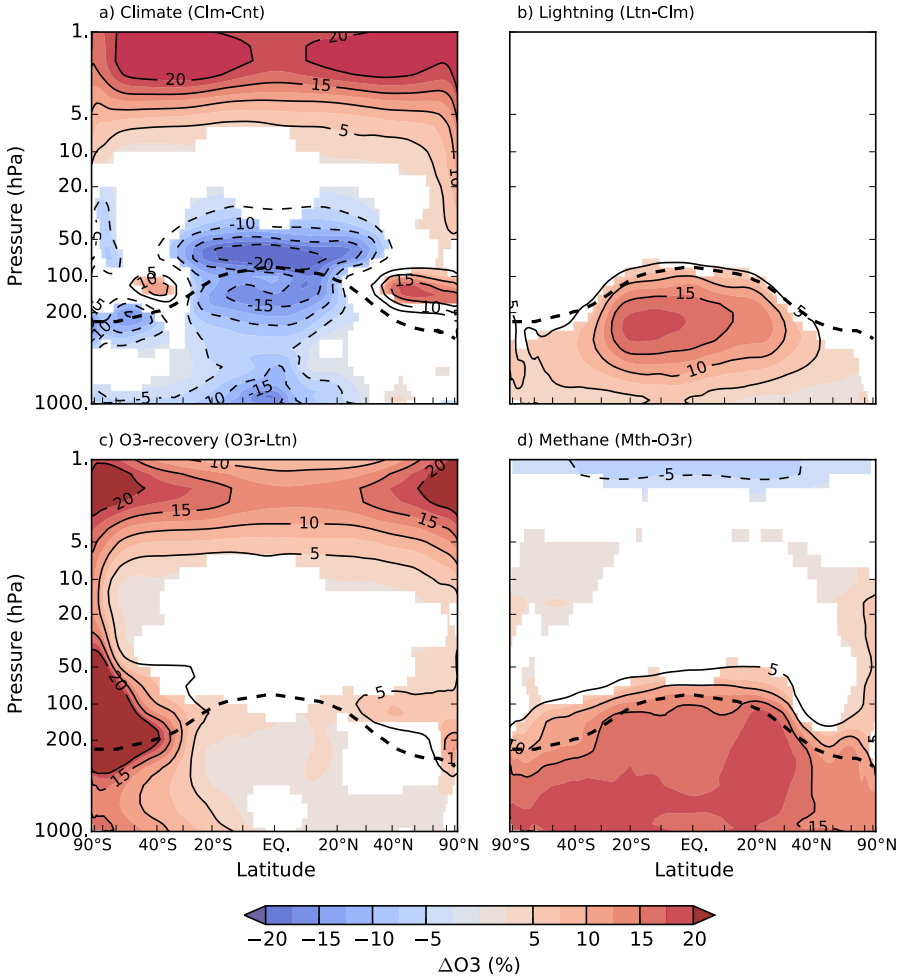

Figure 3. Changes in annual and zonal mean ozone due to (a) Climate (b) Lightning, (c) O3-recovery, and (d) Methane. Contour colours are for statistically significant changes at the 95 % confidence interval using two-tailed Student's t test. The black solid line represents the chemical tropopause based on the Cnt 150 ppb ozone contour.

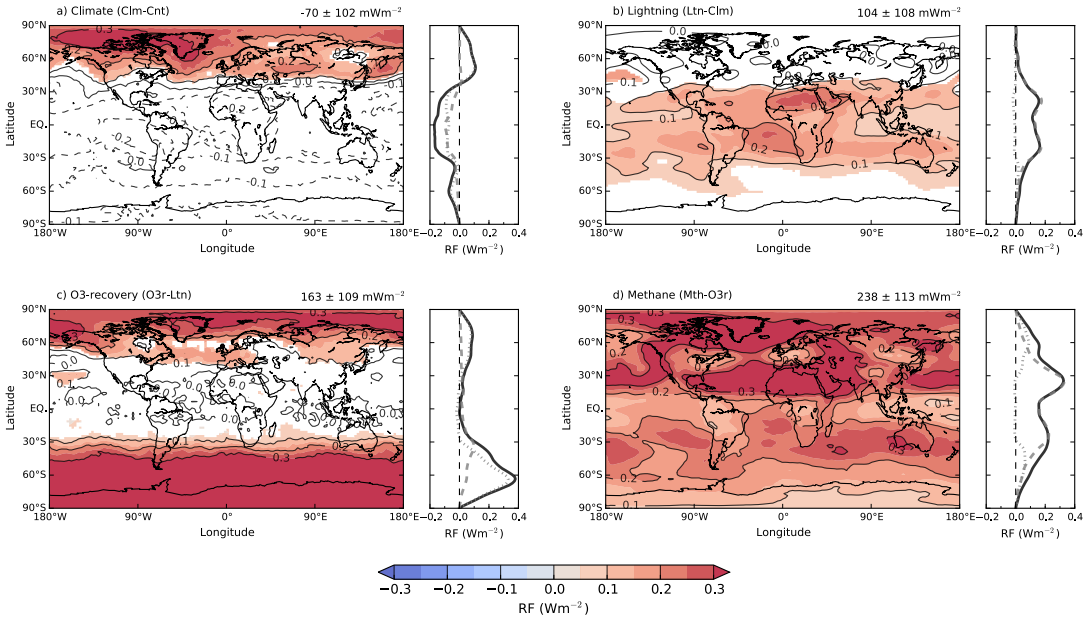

Figure 4. Annual mean maps of ozone radiative forcing (whole atmosphere) due to (a) Climate (b) Lightning, (c) O3-recovery, and (d) Methane. Contour colours are for statistically significant changes at the 95 % confidence interval using two-tailed Student's t test. The annual and global mean is shown on the top right corner (mWm^{-2}). Right panels show zonal mean ozone forcings for the whole atmosphere (solid black), troposphere (dashed grey), and stratosphere (dotted grey). The zonal mean forcings are latitudinally-weighted, i.e. cosine(latitudes).

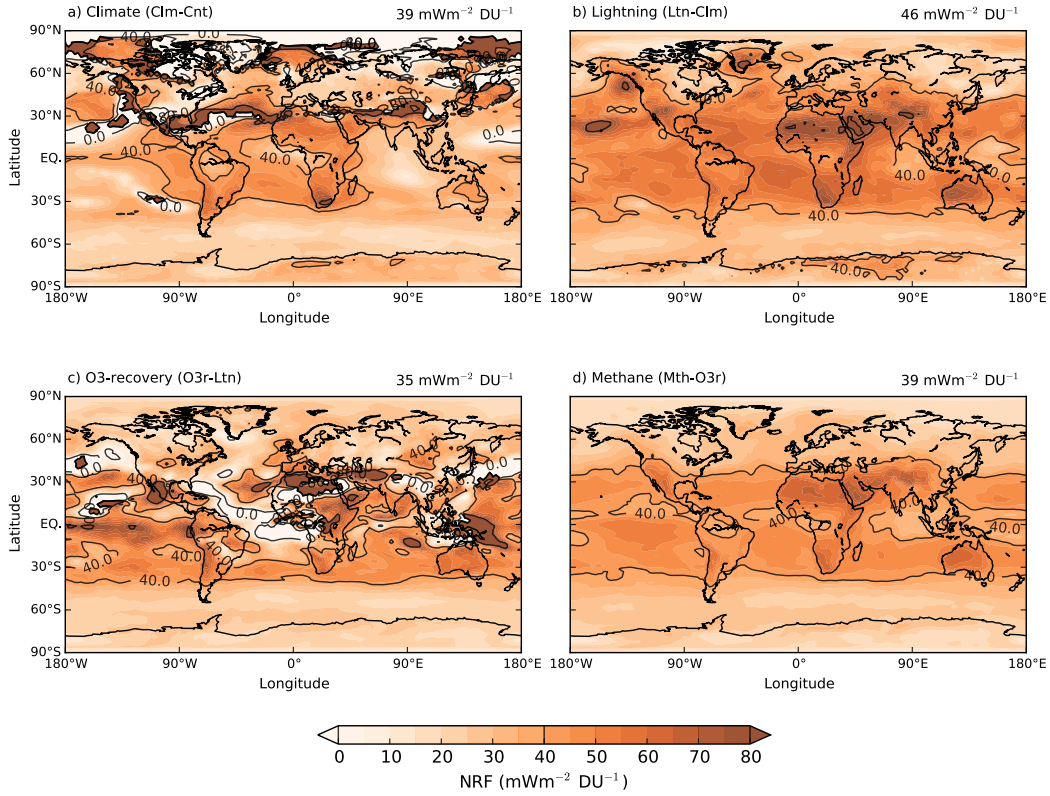

Figure 5. Annual mean maps of normalised tropospheric ozone radiative forcing (i.e. divided by the tropospheric column ozone change) due to (a) Climate (b) Lightning, (c) O3-recovery, and (d) Methane. The annual and global mean is shown on the top right corner (mWm^{-2} DU^{-1}).

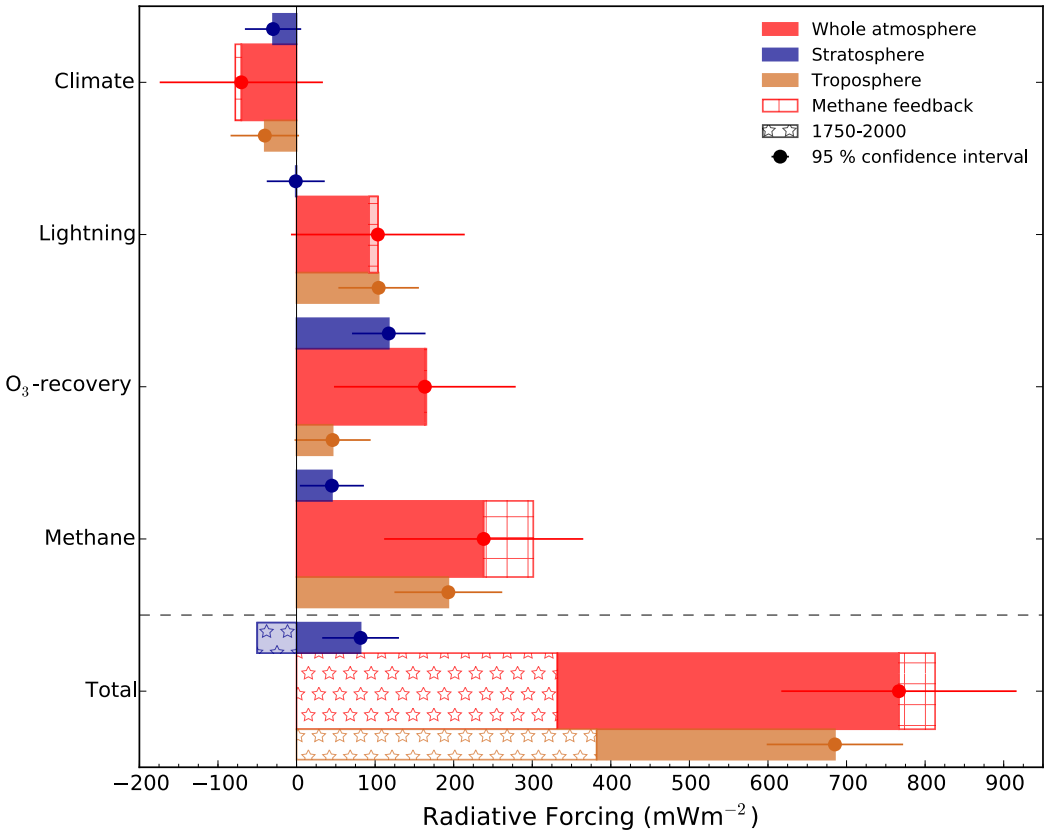

Figure 6. Ozone radiative forcings by drivers (2000–2100; mWm^{-2}). Tropospheric (brown), stratospheric (blue) and net (whole atmosphere, red) forcings are shown. Associated ozone forcings to methane feedback (square-hatched) are shown along with the net forcings. The overall ozone forcing (Total) is the sum of the individual forcings (Climate, Lightning, O_3-recovery and Methane from Table 3) scaled to 1750 (star-hatched). Dots and error bars indicate the mean and the 95 % confidence intervals of the forcings respectively. The information on pre-industrial ozone forcing (1750–2000) and sources of uncertainty are detailed in Sect. 4.